Production of Identified Charged Hadrons vs. Transverse Momentum and Rapidity in $p+p$ Collisions at $\sqrt{s} = 62.4$ and 200 GeV.

I. Arsene,[11,*] I. G. Bearden,[5] D. Beavis,[1] S. Bekele,[10] C. Besliu,[9] B. Budick,[3] H. Bøggild,[5] C. Chasman,[1] P. Christiansen,[5,†] H. H. Dalsgaard,[5] R. Debbe,[1] J. J. Gaardhøje,[5] K. Hagel,[7] A. Jipa,[9] E. B. Johnson,[10,‡] R. Karabowicz,[4] N. Katrynska,[4] E. J. Kim,[10,§] T. M. Larsen,[5] J. H. Lee,[1] G. Løvhøiden,[11] Z. Majka,[4] M. Murray,[10] J. Natowitz,[7] B. S. Nielsen,[5] C. Nygaard,[5] D. Pal,[10] A. Qviller,[11] F. Rami,[2] C. Ristea,[5] D. Röhrich,[8] S. J. Sanders,[10] P. Staszel,[4] T. S. Tveter,[11] F. Videbæk,[1,¶] R. Wada,[7] H. Yang,[8,**] and S.Zgura[6]

(The BRAHMS Collaboration)

[1] *Brookhaven National Laboratory, Upton, NY 11973-5000, U.S.*
[2] *Institute Pluridisciplinaire Hubert Curien CRNS-IN2P3 et Université Strasbourg, Strasbourg, France*
[3] *New York University, New York, NY 10003*
[4] *Smoluchowski Inst. of Physics, Jagiellonian University, Krakow, Poland*
[5] *Niels Bohr Institute, Blegdamsvej 17, University of Copenhagen, Copenhagen 2100, Denmark*
[6] *Institute for Space Sciences, Bucharest, Romania*
[7] *Texas A&M University, College Station, TX 17843*
[8] *University of Bergen, Department of Physics and Technology, Bergen, Norway*
[9] *University of Bucharest, Bucharest, Romania*
[10] *University of Kansas, Lawrence, KS 66045*
[11] *University of Oslo, Department of Physics, Oslo, Norway*

(Dated: April 8, 2013)

The BRAHMS experiment at p+$p$the Relativistic Heavy Ion Collider (RHIC) has measured hadron invariant cross sections for identified charged hadrons for rapidities $-0.2 < y < 3.8$ in $p+p$collisions at $\sqrt{s} = 62.4$ and 200 GeV. The data extends the knowledge of production of soft hadrons at lower c.m. energies corresponding to the highest ISR energy, provides new insight at the highest RHIC energy, and serves as a baseline for the heavy ion measurements.. Transverse momentum spectra are compared to NLO and NLL pQCD calculations and to PYTHIA calculations. Pion spectra are well described by at mid-rapidity and quite well at large rapidities by Next To Leading Order pQCD. The net-proton description from SPS to RHIC energies exhibits longitudinal scaling indicating that not change in stopping mechanism appears significantly in the energy range. The The net-proton rapodoty distributions are not well described by PYTHIA calculation. The rapidity and p_{T}-distributions of pions and kaons are reasonable well described by the PYTHIA8 defaults tunes at 200 GeV.

PACS numbers: 25.75.Dw

I. INTRODUCTION

The scientific program of Brookhaven's Relativistic Heavy Ion Collider (RHIC) benefits from the ability of the machine to collide different species; from polarized protons to heavy ions and asymmetrical collisions like d + A. This versatility has produced measurements that indicate the formation of a strongly-coupled Quark Gluon Plasma (sQGP) in colliding heavy ions [1–4], as well as new insights about the spin of the proton (add references). Seminal results that lead to the characterization of the new medium formed in heavy ion collisions at RHIC as an sQGP are extracted from the comparison of suitable scaled inclusive spectra measured in heavy ion and p + p collisions at the same energy and with the same detectors; deviations from a description of the heavy ion system as incoherent sum of p + p interactions are used to infer the existence of strong partonic energy loss at RHIC [1–4] . This work focuses on the measurements performed in $p+p$ collisions with center of mass energies $\sqrt{s}$= 62.4 and 200 GeV which were run concurrently with the Au+Au and Cu+Cu systems at the same energy. The 200 GeV setting is the maximum that the machine can accelerate Au ions, and 62.4 GeV is an intermediate value between that maximum and previous heavy ion collisions at the CERN Super Proton Synchrotron (SPS), which reached up to 17.3 GeV in fixed target mode. The 62.4 GeV value was also selected to match the highest energy of the $p+p$ collisions at the CERN Intersection Storage Rings (ISR) more than three decades ago.

The data presented in this work was collected with the

*Present Address: ExtreMe Matter Institute EMMI, GSI Helmholtzzentrum für Schwerionenforschung GmBH,Darmstadt, Germany
†Present Address: Div. of Experimental High-Energy Physics, Lund University, Lund, Sweden
‡Present Address: Radiation Monitoring Devices, Cambridge, MA, USA
§Present address: Division of Science Education, Chonbuk National University, Jeonju, 561-756, Korea
¶Spokesperson
**Present Address: Physics Institute, University of Heidelberg, Heidelberg, Germany

BRAHMS spectrometers and spans a wide range in rapidity and transverse momentum. This wide coverage at both energies mentioned above, provide a almost exhaustive description of particle production in $p+p$ collisions, and as such, it complements previous efforts to extract Parton Distribution Functions (PDF) and Fragmentation Functions (FF). In section IV A the different spectra extracted from the two data sets are compared to perturbative Quantum Chromo Dynamics (pQCD) where due to small values of the strong interaction coupling cross sections are actually calculable as series. The comparison between data and these calculations is often used to highlight the partonic nature of the systems that are well described by pQCD. Several publications have addressed particle production in the mid-rapidity region [5, 6] (PHENIX,STAR) where the transverse momentum distributions of pions, kaons and the sum of protons and anti-protons are well described by Next-to-Leading Order (NLO) pQCD calculations . At high rapidity the pQCD calculations continue to describe the charged pion and kaon production [7] (BRAHMS) and neutral pions [8] (STAR) as well, but fail to reproduce the yield of protons.

There is also considerable current interest in understanding the large transverse single spin asymmetries measured with pions and kaons in $p+p$ collisions with center-of-mass energies ranging from 20 to 200 GeV [8–12] Attempts at reaching such understanding are based on pQCD [13] (Feng, Qui Sterman) and it is imperative that such framework be able to describe particle production before engaging in more complicated studies involving spin. Additional high quality measurements of identified charged hadrons at high rapidity at 62.4 GeV will shed light on the validity of pQCD in describing such data.

The spectra presented in this work can also be instrumental in constraining and improving existing event generators. In particular, the widely used PYTHIA model [14, 15] which describes the $p+p$ collisions as unbiased soft particle production or as a sum of the so called underlying event populated by soft particle production and hard QCD processes that appear as jets or high transverse momentum particles. The soft particle production is not yet well understood and needs input from experiment. Much work has gone into tuning PYTHIA at higher energies see e.g. [16]. add some more Rick, LHC Using these data, the event generators will eventually be able to model $p+p$ collisions at all energies ranging from RHIC, the TEVATRON, LHC, and beyond. The present data at $\sqrt{s}$= 62.4 and 200 GeV should constrain these models at energies ranging from the CERN ISR to the Tevatron.

This work reports the study of particle production in $p+p$ collisions at $\sqrt{s}$ = 62.4 and 200 GeV performed with the BRAHMS spectrometers at RHIC. This work is based on the extraction of invariant yields of pions, kaons and their anti-particles as function of transverse momentum in different rapidity windows. The collisions at $\sqrt{s}$ = 62.4, where the beam rapidity is equal to 4.2, have been studied at $y = 0$ and 1, and in the interval 2.2-3.8 For the higher energy collisions where $\sqrt{s}$ = 200 GeV and beam rapidity is equal to 5.4, the coverage in rapidity is wider: y=0-1.2 and y=1.6-3.8.

This paper is organized as follows: Section II discusses the BRAHMS detector system as it was setup for the $p+p$ runs. Additional details are included for three subsystems which were not dexcribed in previous BRAHMS publications. The same section describes the data analysis in different sub-sections starting with a detailed description of the tracking algorithms used in both spectrometers, followed by the identification of the detected charged particles. Cross section extraction and the corrections applied to the data during that process are also described in this section which ends with a summary of the systematic uncertainties that are estimated to be present in these studies. Section III is a thorough description of the results, starting with the transverse momentum distributions and particle ratios, followed by a comparison of the $\sqrt{s}$ = 62.4 spectra to corresponding measurements performed at the ISR. This section then proceeds to describe the rapidity distributions of the yields and the average mean transverse momentum. The presence of Longitudinal Scaling in these data is investigated, the degree of stopping is studied using the rapidity distribution of net protons. Strangeness production in $p+p$ collisions is presented as function of the anti-proton to proton ratio as proxy of the baryon chemical potential. And finally section III presents the energy dependence of the average multiplicity. Section IV describes the comparison between the invariant yields extracted from $p+p$ collisions at $\sqrt{s}$ = 62.4 and 200 GeV, and NLO pQCD calculations. Similar comparisons with PYTHIA 8 calculations are also presented for the 200 and 62.4 GeV data.

.

II. ANALYSIS

The data used for this analysis were collected with the BRAHMS detector system during the 2005 and 2006 RHIC runs. The 200 GeV $p+p$ data matches previous heavy ion runs which collected data from Au+Au and Cu+Cu collisions. The lower energy data ($\sqrt{s}$= 62.4 GeV) was collected during a short run in 2006. The experiment sampled $0.26pb^{-1}$ of $p+p$ collisions at 62.4 GeV and $3.4pb^{-1}$ at 200 GeV.

A. Detector System

The BRAHMS detector consists of two movable magnetic spectrometers: the Forward Spectrometer (FS) that can be rotated from 2.3° to 15° , and the Mid-Rapidity Spectrometer (MRS) that can be rotated from 34° to 95° degrees relative to the beam line. Several global detectors are also used to measure the multiplicity of charged particles, the luminosity at the iteraction region, and to determine the interaction vertex. The vertex finder detector provides as well a precise start time for time-of-flight measurements in both spectrometer arms.

The MRS is a single-dipole-magnet spectrometer with a solid angle of $\approx 5msr$ and a magnetic bending power up to 1.2 Tm. The MRS has two Time Projection Chambers (TPCs), TPM1 and TPM2, situated in field free regions in front and behind the dipole magnet. This assembly is followed by a two highly segmented scintillator time-of-flight walls, the first one refered as TOFW is located at 4.51 m and the second one named TFW2 sits 5.58 m (at the 90° spectrometer setting) or it can be moved out to 6.13 m (all other MRS angle settings).

The FS consists of 4 dipole magnets D1, D2, D3 and D4 with a total bending power of up to 9.2 Tm. The spectrometer has 5 tracking stations T1 through T5. T1 and T2 are TPCs placed in front of and after the second dipole D2. T3, T4, and T5 are drift chambers with excellent position resolution ($\approx 80\mu m$) with T3 in front of D3, T4 between D3 and D4, and T5 after D4 and just in front of the particle identification detectors H2, which is a segmented time-of-flight wall and the Ring Imaging Detector (RICH) [17]. The D1-D4 magnets are all set to run at the same fraction of their full field value. Thus the acceptance for a given settings picks a certain momentum range around a p_{ref}, a reference momentum. At the highest field setting the p_{ref} is 22 GeV/c. The momentum resolution is dominated by the position resolution of the tracking detectors, and can be expressed as $\delta p/p = 0.016p/p_{ref}$, implying the resolution is no worse than $\approx 2\%$ for accepted particles of interest at any given setting.

Additional details on the BRAHMS experimental setup can be found in Ref. [18] and in Ref. [19] for tracking in the MRS. This paper describes three detectors subsystems not discussed in the references mentioned above; namely the vertex and luminosity detectors installed for $p+p$ running, the extended time-of-flight wall (TFW2) in the MRS, and the spectrometer trigger counters used in the BRAHMS experiment for Run-4 through Run-6.

1. *Vertex and Luminosity detectors*

A set of four Cherenkov Counters (CC) installed at 1.9 (inner ring) and 6.4 meters (outer ring) on both sides of the nominal interaction point (IP) are used to measure the luminosity. Because these detectors were designed to achieve good time resolution, they also provide a measurement of the vertex of the collision and the start time for time-of-flight measurements. Each detector consists of a 4.87 cm thick Lucite radiator backed by a small number of Photo-Multipliers Tubes (PMTs) (8 and 5 in inner rings, 10 in the outer rings). The light collection in these detectors is such that most of the Cherenkov light emmitted by incident charged particles above threshold will reach the PMT photo-cathode but some fraction will be lost, a fact that complicates the sue of these counters for charge particle counting. In contrast, these detectors have very good timing resolution and are highly efficient. The detectors covers the pseudo-rapidity range from $3.26 < \eta < 5.15$. The left inner and outer rings, and the outer right ring have full azimuth coverage, while the inner right ring has a cutout for $120° < \phi < 240°$ to minimize background production into the FS. An average timing signal is derived from all tubes hit in the left and right array. The sum and the difference of these represents the start time of the event and the vertex position of the interaction. From comparisons to vertices formed with tracks measured in the MRS spectrometer we deduce that the position resolution is ≈ 1.2 cm, which corresponds to a time resolution of about 100 psec.

There are significant yields of charged particles in $p+p$collisions at 200 GeV within the rapidity coverage of the CC detectors. This produces a fairly high efficiency to detect coincidences between the two sides; these detectors are estimated to be sensitive to $\approx 68\%$ of the total inelastic cross section of 41 mb. For $p+p$collisions at 62.4 GeV the beam rapidities are smaller and the CC detectors are only sensitive to $\approx 33\%$ of the total inelastic cross section (36 mb) and 45% of the Non-Single-Diffactive (NSD) cross section.

Further details about design and performance of the CC detectors can be found in a technical paper [20].

2. *TFW2*

The TFW2 detector is an array of 41 BC408 scintillator slats designed to measure time-of-flight of charged particles in the MRS. each slat is 40 cm high, 5 cm wide and 1.5 cm thick coupled with optical cement at both ends to H2431 PMTs (2 inch Hamamatsu R2083 assembly). The anode signal is passively split and one signal is feed to a FASTBUS ADC, while the other is connected to a discriminator for timing purposes. The input signal to the discriminator is passed through a low frequency filter mounted right at the tube base. This detector is built to be symmetric about the axis of the MRS and can move radially between XXX and YYY cm measured from the pivot of the spectrometer. The scintillator slats are mounted on two arcs. The front arc has a radius of curvature of 508 cm and the back one has a radius of 512 cm, both arcs are centered in the D5 nominal center whenever the detector is at the shortest distance to the spectrometer pivot. In the extended position the nominal path length 614 cm [THIS IS NOT CORRECT] The overall time-resolution of the detector system is 120 psec.

3. *Triggers*

The MRS trigger is formed by requiring coincidences between the time-of-flight (TOFW) wall placed at 4.33

m from the IP, a hodoscope (TRMRS) placed immediately behind the D5 magnet, and the RHIC 9.7 MHz clock. The TRMRS is a 12 slat scintillator hodoscope, each with dimensions $2\times9\times0.4$ cm (W*H*D) read out by fast phototubes (XXXX) at both ends of each slat. The slats were made thin to minimize the multiple scattering for low momentum particles. Details about the TOFW detector can be found in ref. [18]. A PMT signal from both TOFW and TRMRS detectors was fed into custom designed programmable VME modules where each channel has a discriminator circuit that provides an ECL output. These modules require a coincidence overlap between the input from the top and bottom signal from each scintillator slat and then provides a logic OR of all 16 slats connected to it. The overlap coincidence time is 20 nsec. A set of such modules are daisy-chained to form the logic requirement of one good hit in the the respective hodoscope. The resolving time of the TOFW and TRMRS detectors is much smaller than the bunch crossing time of 107 nsec.

In the FS, the trigger is formed with signals from a hodoscope (TRFS) placed immediately behind the magnet D1 and in front of the first tracking detector T1, and the two time-of-flight walls H1 and H2, placed at 8.8m and 18.8 m, respectively, as well as the RHIC 9.7 MHz clock. The TRFS is a 7 slat hodoscope with slat dimensions $3\times9\times0.4$ cm (W*H*D) readout by fast phototubes (XXXX) at each end a similar in design as the TRMRS. The triggers in both spectrometers do not require the minimum bias CC trigger, and thus register tracks from events that are part of the total inelastic $p+p$ cross section, including single diffractive and double diffractive events. The efficiency of both spectrometer triggers have been estimated using minimum bias data sets, and were found to be greater than 98%. The enhancement factor for these triggers are large: $\approx 100-1000$ depending on angle and field setting due to the small solid angle of the spectrometers. For the FS the largest luminosities seen in 200 GeV $p+p$ produced event rates of 4-100/sec, which were handled by the DAQ with dead times $\leq 25\%$. For the MRS the data were usually downscaled by factors of 3 to 5 in order to maintain good live time for the FS. The dead time is dominated by the readout time of the TPCs.

B. Tracking

Local tracks are first determined in the TPCs and Drift Chambers, which are all situated in magnetic field free regions. The resulting straight-line track segments in two tracking chambers located on either side of a magnet are matched using the effective edge approximation. The rigidity of the matched track p/q is determined by:

$$p/q = \frac{Bl}{(sin(\phi_b) - sin(\phi_f))\sqrt{(1-\alpha_y^2)}},$$

where Bl is the integrated effective field, ϕ_f the angle between the tangent of the curvature in front of the magnet at the position of the effective edge, ϕ_b is the same quantity at the back end of the magnet, and α_y the average of the vertical slope of the track. The magnetic field inside D4 magnet gap has a spatial non uniformity which requires a second correction to the deduced momentum. The correction depends on the orbit of the track and it was deduced from full Geant simulations of the spectrometer using a field map generated by the TOSCA program set to match the measured D4 field. Local tracks and local matched tracks are combined in the FS to form complete tracks. Complete tracks are refitted to deduce the final value of momentum. Tracks in the FS are required to project through the magnet D1 onto the nominal beam-line.

A number track quality cuts are applied to select good tracks. The magnitude of related corrections and the evaluation of systematic errors arising from them are discussed later in section II H 1

bulleted list may not be appropriate for PRD

- Matching of local tracks between the tracking chambers i.e. TPCs and Drift Chambers. When using the effective edge approximation a cut based on the horizontal angle difference, and the angle and position difference in the vertical plane. Whenever tracks reconstructed in the T2 TPC and the T3 drift chamber are matched, the absence of magnetic field between those detectors calls for a different approach and a six sigma elliptic cut in x y, δx , δy is applied. The means and the RMS of the distributions used in the track matching are determined from data on a run-to-run basis in a pre-pass of the global tracking.
- Fully reconstructed tracks are extrapolated back to the primary vertex. The intercept of the extrapolated track and the beam axis is compared with the z coordinate of the vertex which was measured with the CC detectors. In case no CC vertex was found for a particular event, beam-line constraints are applied in the transverse coordinates x and y.
- Magnet fiducial cuts requiring clearing the physical boundaries by 1 cm.
- Fiducial cut on the last PID detector. For the FS this is the RICH detector where the thin walled window have a dimension of 40×20 cm^2, or the H1 active slat range. For MRS is it the chosen active slat in TFW2.
- Whenever particle identification is done using Time-of-Flight, tracks are matched to hits in the TOF walls. a track is accepted if it projects to a slat that has signal or its inmediate neighbor. A three sigma match in Y position is also required. The y coordinate of a hit in a particular slat is determined from the time difference between signals from the corresponding top and bottom PMTs.

Tracking and matching efficiencies for each of the five tracking stations in the spectrometer were calculated by constructing full tracks using just 4 track segments and evaluating the efficiency in the 5^{th} station by comparing the predicted position and direction of the interpolated or extrapolated full track in that station with the known local segments. The local track efficiency as function of position and direction of the track segments was evaluated at each spectrometer angle and field setting. The overall tracking efficiency is about 80-90%, and is included in the extraction of the cross sections.

C. Particle identification

In MRS the particle identification is done using the time-of-flight with the CC time as start and the TFW2 (or TOFW) time as the stop. The TOFW time-of-flight was used for checking result from TFW2. Due to the longer flight path whenever the TFW2 is used, the momentum range for good particle identification can be extended at the cost of a small reduction in yield due to additional decay and absorption of particles.

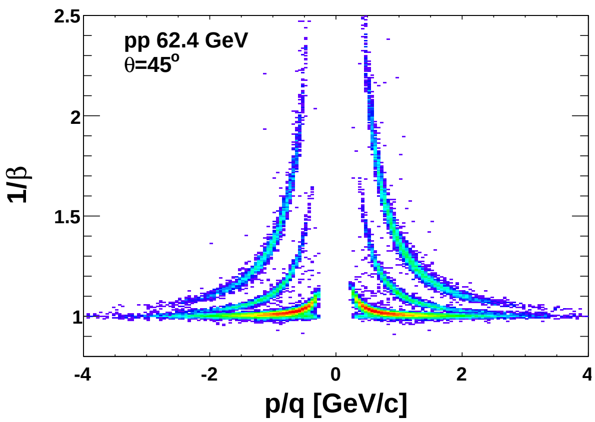

FIG. 1. (Color online) $1/\beta$ vs. p/q with MRS at 45°.

To identify charged pions, kaons and protons using the time-of-flight detectors three standard deviations σ cuts in $1/\beta - 1/\beta_C$ where $\beta_C = |p|/\sqrt{p^2 + m^2}$ is the calculated velocity and β the measured velocity. A typical correlation between velocity and momentum of charged particles detected in the MRS spactrometer at 45° is shown in Fig. 1 and it demonstrates the overall good particle identification in the MRS It is noted that in order to make the PID with time-of-flight an event vertex and a start time signal from the CC counters are needed. This has important consequences for the normalization as is discussed later. The resolution in $1/\beta$ for TFW2 has an average values of 0.0055 at 45° and 0.007 at 90°. With these resolutions kaons are well separated from pions up to 1.8 GeV/c, while protons are separated from kaons up to 3 GeV/c. The pion spectra can be extended to somewhat higher momenta since the K/π ratio is well below 1 ($\approx 0.2 - 0.35$). An analysis in which slices were made in the $1/\beta - 1/\beta_C$ distributions for momenta above 1.8 GeV/c was used to extract the ratio of K/π vs. momentum at 90° and 45°, and to estimate the contamination from kaons in the pion spectrum within the 2.5σ cut. Below 1.9 GeV/c the contamination is negligible, but grows to typically $\approx$ 30% for π^+ at 2.6 GeV/c and to 25% for π^- at 2.7 GeV/c. Spectra of pions are presented from the 90° setting up to $p_{\rm T}$= 2.8 GeV/c and at 45° setting up to $p_{\rm T}$= 2.2 GeV/c.

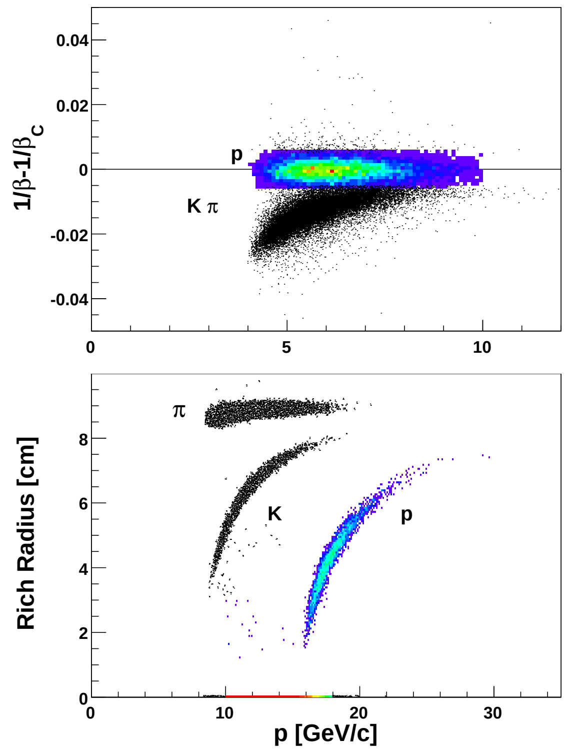

FIG. 2. (Color online) Top panel: Particle identification at 6°. Bottom panel: PID using RICH at 3° and half field.

In the forward spectrometer the particle identification is made primarily with the RICH detector, and with H1 and H2 time-of-flight walls at lower magnetic field settings. For all angle and field settings the pions are above the threshold in the RICH, and are identified requiring that the measured ring radius is within 3σ of the calculated radius on a track-by-track basis. The yields are corrected by the RICH efficiency, which decreases near the threshold due to fewer Cherenkov electrons emitted. The efficiency is estimated from data using the time-of-flight measured in H2 and from a detailled GEANT based detector simulation of the RICH as described in Ref. [17]. Kaons are identified in the momentum range $10 < p < 20$ GeV/c using the same technique, with the additional requirement that the measured radius is more than 3σ away from the pion radius at a given momentum. The efficiency of the RICH detector has been studied with pions identified with a scintillator time-of-flight counter in an overlapping momentum range and reaches an upper value of 97%. Protons and anti-protons are identified using the RICH in veto mode in the momentum range $10 < p < 18$ GeV/c: protons will not produce a signal in the RICH; most pions and kaons in this momentum range will emit Cherenkov light, but a small fraction typically $\approx 2.8\%$ leaves no signal. This inefficiency may be due to interactions, or secondary scatterings after the H2 hodoscope. The contribution from these events mimicking as protons is subtracted on a statistical basis from the protons candidates assuming they constitute 2.8% of the measured pions and kaons in the same setting. For protons this correction is very small, but for anti-protons it results in a roughly 50% systematic uncertainty on the yields at the highest rapidities at 62.4 GeV, and considerable lessbe specific for the 200 GeV data. In the momentum range $3 < p < 8$ GeV/c i.e. for the 4°-12° settings protons and kaons are identified using the time-of-flight in H2 and requiring that no signal is observed in the RICH. The purity of the proton sample can be estimated from data, and the kaon contribution per momentum bin is determined from fitting the timing distribution with multiple Gaussians and subtracting the contamination in the final analysis. The quality of the PID separation of protons from kaons and pions is illustrated in Fig. 2.

D. Data Sets

The BRAHMSs spectrometers were run independently, data-taking is best characterized by the angular and magnetic field settings of each spectrometer. The data taken for 200 GeV are summarized in table I and the data taken for 62.4 GeV are summarized in table II, These tables list the number of collected events at different spectrometer angles, and magnetic fields listed as the fraction of the maximum value. An effort was made to collect a similar number of events for both polarities of the magnets. In the FS positive particles are accepted for the A polarity, while B polarity accepts negatives. Since the second goal of the experiment at both 200 and 62.4 GeV was to measure transverse single spin asymmetries for identified charged hadrons at large values of x_F in the forward region the largest fraction of the beam time was devoted to the 3° and 2.3° settings for the FS.

Spectrometer	Angle	Field	A Pol Trig	B Pol Trig
MRS	90	0.16	1390	-
	90	0.31	690	-
	90	0.47	3510	970
	90	1.00	2890	5760
	60	0.31	260	320
	45	0.31	700	-
	45	0.47	6140	7830
	40	0.31	490	170
	34	0.31	1930	1250
	34	1.00	5870	3140
FS	8	0.18	140	370
	8	0.35	30	60
	8	0.50	30	60
	8	0.71	30	30
	4	0.12	190	220
	4	0.25	430	520
	4	0.35	230	60
	4	0.50	300	520
	4	0.71	360	190
	4	1.00	1080	1230
	2.3	0.25	720	1660
	2.3	0.50	680	550
	2.3	1.00	15220	33030

TABLE I. Angles, field settings and number of triggers in tousands (k) for data taken at $\sqrt{s_{\rm NN}}$= 200 GeV. The field value is given as the fraction of the maximum for D1 and D5 in FS and MRS, respectively.

Spectrometer	Angle	Field	A Pol Trig	B Pol Trig
MRS	90	0.16	810	-
	90	0.31	1310	310
	90	0.47	-	90
	45	0.31	2350	-
	45	0.47	3490	-
FS	6	0.25	230	360
	4	0.18	500	1100
	4.0	0.50	-	110
	3	0.50	640	2020
	2.3	0.50	1400	1030

TABLE II. Angles, field settings and number of triggers for data taken at $\sqrt{s_{\rm NN}}$= 62.4 GeV

E. Cross Section determination

The differential cross section for hadron production is calculated from the minimum bias data, or from the triggered data set where the minimum bias condition is required, as

$$E\frac{d^3\sigma}{dp^3} = \mathcal{L}^{-1}\frac{1}{2\pi p_T}\frac{1}{f_h}\frac{1}{A_c\epsilon_{rec}}\frac{\rm N_h}{\Delta p_T \Delta y} \quad (1)$$

where $\mathcal{L}$ is the integrated luminosity for a particular data set, $\rm N_h$ the number of counts in a given $\Delta p_T \Delta y$ wide bin at a $p_{\rm T}$-value; The f_h is the fraction of the inclusive hadron yield where the minimum bias condition is satisfied(same notation as in Ref. (Phenix pp). The acceptance correction is given by A_c and all the efficiencies associated with the hadron tracking and particle identification are included in the ϵ_{rec} factor. For the triggered only data set, the factor f_h is 1. We discuss in greater detail in the subsequent section how each of these factors are determined.

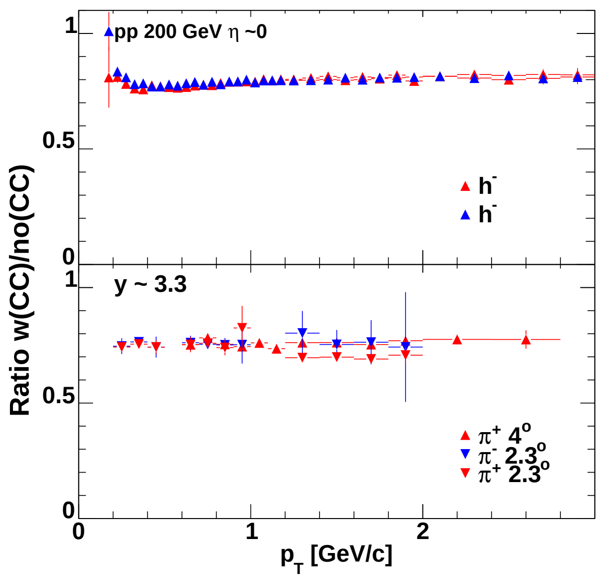

FIG. 3. (Color online). Ratio of charged hadron cross section for event classes with and without a CC-vertex at 200 GeV, at mid rapidity (top) and identified pions near rapidity 3 (bottom).

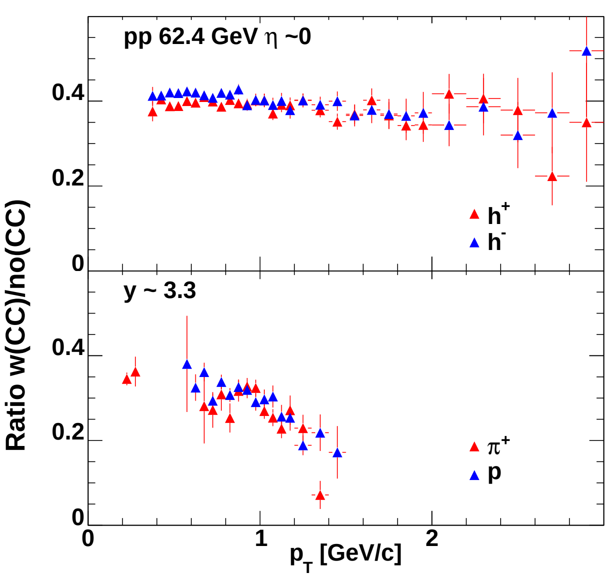

FIG. 4. (Color online) Ratio of charged hadron cross section for event classes with and without a CC-vertex at 62.4 GeV, at mid rapidity (top) and identified pions near rapidity 3 (bottom).

F. Luminosity Determination, Normalization and trigger bias

The luminosity is deduced from the measured counts with the CC counters from minimum bias data using $N_{cc} = \mathcal{L}\sigma_{CC}$. The minimum bias CC trigger requires a minimum of one hit in each side of the CC detector system. The accepted vertex range measured whith those detectors covers the full interaction region from -150 to $+150$cm. The σ_{CC} was evaluated using the method of Vernier scans [21]. Details for the scans performed at 62.4 and 200 GeV are given in the following subsections. It is noted that the systematic uncertainties in the normalization between the 62.4 and 200 are mainly un-correlated since they are derived from two independent measurements.

1. 62.4 GeV

The σ_{CC} was evaluated from two separate Vernier scansand is found to have the value of 12 ± 1.4 mb. This correspond to about 40% of the NSD cross section of 27 mb and $\sim$ 33% of the total inelastic cross section of 36 mb.

Therefore, there is a bias towards selecting events with a high multiplicity of particles when the global vertex is required for event selection. This in general is avoided by having spectrometer triggers that do not require the vertex information. A correction though is needed where the PID is done with time-of-flight both in the MRS and in the FS, since the start time is derived from the CC coincidence data. In contrast when identifying particles based on the information in the RICH detector no such bias is introduced. This bias can also have a $p_{\rm T}$-dependence. This p_T-dependence was evaluated for the forward spectrometer settings from the data using RICH information only comparing $p_{\rm T}$ spectra with and without the requirement of a global vertex. In the MRS it was evaluated using h^+ and h^- and comparing spectra with and without the vertex requirement to be less than a 10% effect. It was also checked for π in the $p_{\rm T}$-range < 2.0GeV/c using the MRS trigger counter as the start detector. In the MRS the effect is quite small for $p_{\rm T} < 3.0$ GeV/c, and in the FS for $p_{\rm T} < 1$ GeV/c which covers the majority of settings where time-of-flight is used. The effect is demonstrated in Fig.4 where we plot the ratio of cross section requiring the CC vertex over yield of events with no such requirement *i.e.* the the hadron fraction f_h needed for the cross section calculation. The top panel shows this for MRS at 90° for positive and negatively charged hadrons, and in the bottom panel for pions at forward rapidities. Note that here the reduction at large $p_{\rm T}$ is clearly due to exhausting the available energy for particle production. It is assumed f_h is constant for $p_{\rm T}$ less than 0.8 GeV/c. Fortunately, the majority of data at higher $p_{\rm T}$ comes from the RICH PID and the vertex information is not required, but the inelastic cross sections are determined directly.

2. 200 GeV

For the 200 GeV data analysis we required in the analysis that the event had a CC vertex associated with it, both at mid-rapidity and forward rapidity. Therefore the experimentally measured cross section is the invariant yields for the NSD. The in-elastic cross section can be obtained using eq. 1 with the additional knowledge of the σ_{CC} and the factor f_h. Unfortunately, we do not have a precise vernier scan measurement, but only a value of $\sigma_{CC} \sim 28 \pm 3.5$ mb i.e. 15% uncertainty. The efficiency of the CC counter were also estimated by Monte Carlo simulation using PYTHIA events as input. This resulted in an estimated cross section of $\sim 27.5 \pm 2$ depending on the tunes selected consistent with the vernier scan measurement. Figure 3 shows the ratio f_h for the 200 GeV data at y$\sim$ 0 and high rapidity. At this energy we do not observe any p_{T}-dependence up to 3 GeV/c consistent with the observation by PHENIX for π^0 production at mid-rapidity [22] where no p_{T}-dependence was observed up to 10 GeV/c. The yields obtained requiring the CC vertex can be equated with the NSD density distributions, and the density distributions for the total inelastic cross sections can be obtained from the by a multiplicative factor of 0.82 at mid-rapidity and 0.87 at forward rapidity.

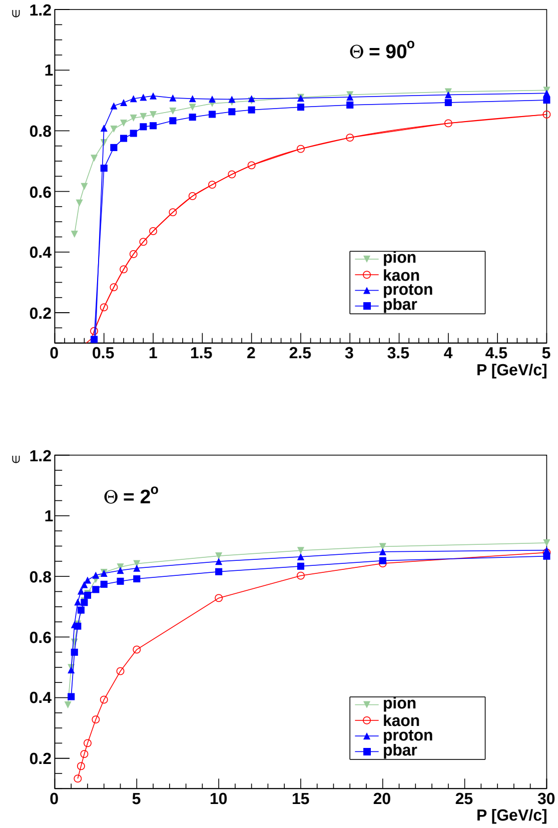

FIG. 5. (Color online) Efficiency of singles particles of pion, kaons and protons in the MRS (top panel), and in the FS at 2° (lower panel).

G. Corrections

The data are corrected for the geometrical acceptance of the spectrometers, multiple scattering, weak decay of pion and kaons, and absorption in the material along the path of the detected particles. It is assumed that the geometric acceptance and the correction due to the different physical processes that particles are subject to, can to first order be factorized. I has been confirmed by full Monte Carlo simulation with simulated input spectra having similar p_{T}-shapes as the observed spectra that this procedure reproduces the input spectra to better than 2% overall. An exception is observed at mid-rapidity where deviation are seen for protons with momenta less than 0.7 GeV/c, kaons less than 0.5, and pions less than 0.4. An additional correction based on this calculated difference is applied for the low momentum mid-rapidity data. It is primarily caused by reduction of yield due to multiple scattering out of the MRS acceptance at low momenta. In the forward spectrometer no such additional correction was found to be needed. The BRAHMS spectrometers are small solid-angle devices so the largest correction to the recorded yield is from geometrical acceptance of the spectrometers. It is evaluated by a purely geometric Monte Carlo procedure, that is equivalent to what is used for the more sophisticated analysis based on detailed and complete Geant simulations. Particles are thrown from different vertex positions along the beam line where interactions take place, sorted into vertex bins of 5 cm, and we record the probability that the particles traverse the spectrometers at any given field setting, and are hitting the fiducial volumes in questions i.e the TFW2 wall, the RICH detector, or the H2 hodoscope. For each particle kind we keep a record of this probability as function of y and p_{T}. The vertex bin size is slightly larger than the resolution of the CC counters and deduced cross section were insensitive to using a smaller bin-size. The accuracy of this correction is better than 1.5%, so even though it is large in order 50-200, it is very well determined.

The correction due to the interaction and decays particles experience in the spectrometers is evaluated as follows. For each kind of particle π, kaons, protons, and anti-protons the correction is determined as function of momentum and spectrometer angle setting using the BRAG (BRAMS Geant) program that is based on the GEANT3 libraries [23], describing the BRAHMS detector system. The default physics modes and parameters and cuts are used. The hadronic interaction are evaluated using the GEANT-FLUKA interface [24]. For $\bar{\mathrm{p}}$ at low momenta there is a significant difference compared to the default GHESIA interface, while corrections for other particles are within 1% using the two different packages. We have compared to p̄-absorption data showing that GEANT-FLUKA provides a better description of this annihilation process at low momenta than the default GHESIA hadronic description in GEANT3. Single particle are tracked by BRAG, the hits in the detectors are digitized and subjected to the same analysis package as real data. The accuracy of these corrections is estimated to be $\approx 1\%$ (absolute) on corrections typically $85-95\%$, on top of the trivial decay correction for pions and kaons. In Fig. 5 we show this correction as function of momentum at 90° and 2°. The dominant effect in FS is from hadronic interaction in the spectrometer path including the Be beam-pipe.

H. Vertex Dependences

As mentioned above the acceptance is vertex dependent. In addition there are effects due to the low statistics that must be taken into account when calculating the invariant cross sections σ_{y,p_T} are calculated from the number of counts in a y-$p_{\rm T}$ bin, $N(y,p_T)$ from Eq.1.

Since the vertex distribution of $p+p$ collisions is rather wide ($\sigma_Z \approx 60cm$ and the spectrometer acceptance depends on the vertex position, most strongly for the MRS, the specific sums are using the following equation:

$$\sigma_{y,p_T} = \mathcal{L}^{-1} \sum_v N(y,p_t,v) / \sum_v 2\pi p_T \; A_c(v)\epsilon_{rec} \qquad (2)$$

This particular summing preserves the proper Poisson statistics in case of bins within acceptance, but with 0 counts which is important at larger values of p_T and low statistics (y,p_T) bins. A detailed description of this can be found in [25].

Due to the small acceptance of the FS a fair number of y-$p_{\rm T}$ bins lies on the edge of acceptance. We reject bins where the acceptance is less than 60% of the average bins in the rapidity range for a given setting. In additions since the data are analyzed in small bins (typically 50MeV/c*0.05(rapidity), and results are presented in larger bin, corrections due to the covered $p_{\rm T}$-range (from acceptance) compared to the average (for the bin) has to be taken into account. This is done by correcting the yield based on the value of the $p_T^{covered} - p_T^{average}$ and using the mean slope of the $p_{\rm T}$-spectrum for a particular rapidity bin. At the highest rapidity and the smallest field settings this correction can be up to 15%. Since the cross sections also change with rapidity a similar corrections in this variable could be performed, but in all cases it is estimated to be less than a few percent and has been ignored.

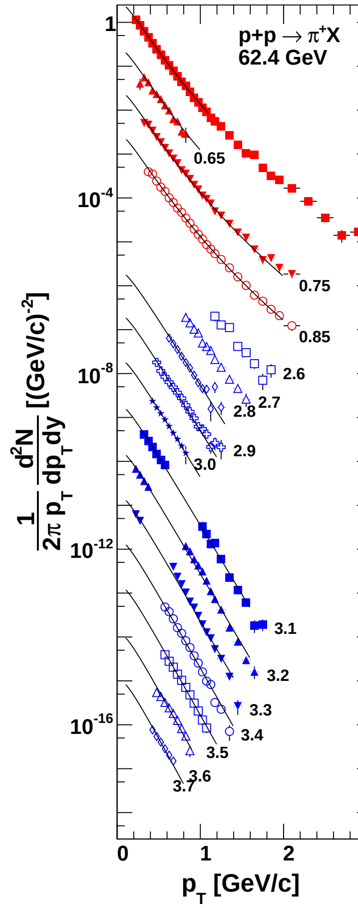

FIG. 6. (Color online). Invariant transverses $p_{\rm T}$-spectra for π^+ (left) and π^- (right) at 62.4 GeV for rapidities as indicated in the figure. Each rapidity bin is scaled down by a factor of 10 from the previous. The first four spectra are from MRS (red online).

1. *Systematic uncertainties*

The spectrum data have been corrected for several effect, some of which have been discussed in the previous sections. In the section we summarize the effects, typical values and estimates of the systematic uncertainty associated with each.

- Yield corrections from tracking, efficiencies in tracking detectors, matching efficiencies matches of spectrometer tracks to the beamline and/or vertex determined by the CC counters.
- Geometric acceptance.
- PID corrections. Intrinsic efficiency of the RICH or Time-of-flight detectors, efficiency of matching of tracks to hits.
- Corrections for losses due to Nuclear interactions, multiple scattering, weak decays of π and kaons.

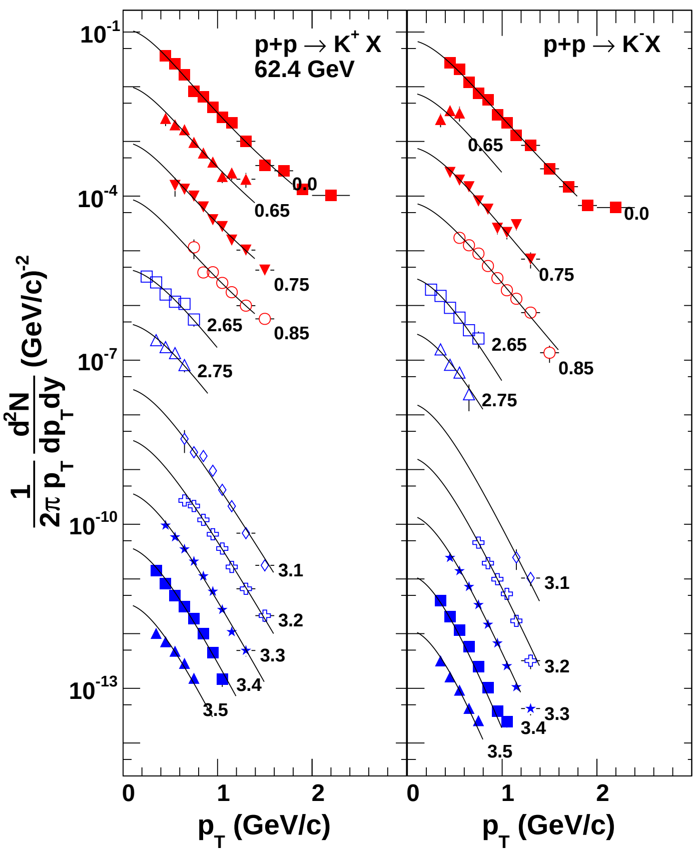

FIG. 7. (Color online) Invariant rapidity densities for K^+ and K^- for rapidities as indicated in the figure Each rapidity bin is scaled down by a factor of 10 from the previous

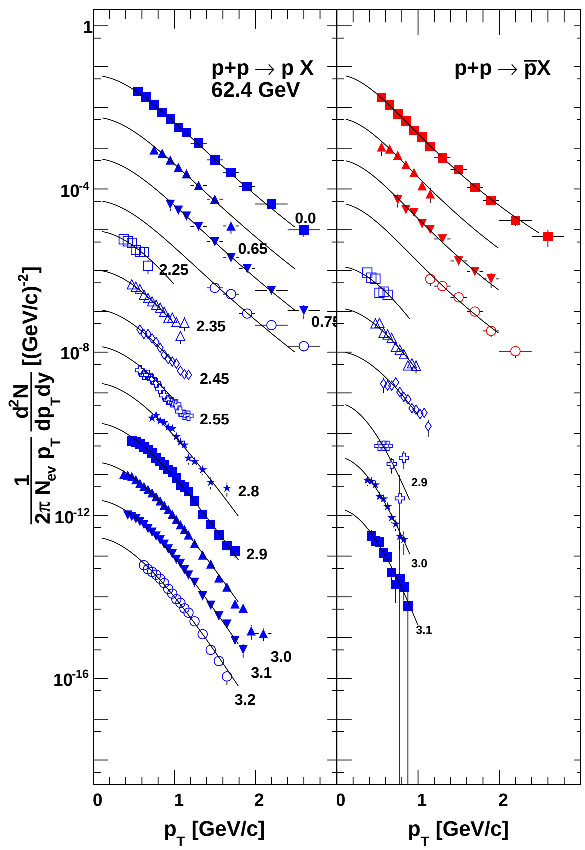

FIG. 8. (Color online) Invariant transverse p_T spectra for protons and anti-protons for rapidities as indicated in the figure. The spectra for each rapidity bin is scaled down by a factor of 10 from the previous.

- Uncertainties in determinations of events normalization, including effect of Vernier scans.
- Run Normalization and Vernier Scan.

The systematic uncertainties on the p_T spectra shown in this chapter arise from the cuts and corrections applied to the data.

III. RESULTS

A. Transverse Momentum Spectra

The invariant spectra for pions produced in 62.4 GeV collisions are shown in Fig. 6, the corresponding distributions for kaons are shown in Fig. 7, and the ones for protons and anti-protons are shown in Fig. 8. The invariant cross sections are normalized to the total inelastic cross section of 36 mb. For clarity in each figure, the spectra extracted at different rapidity bins, are scaled down by a factor of 10 starting at mid-rapidity. The average rapidity value in each bin is listed on the right of each spectrum.

The invariant spectra extracted from 200 GeV $p+p$ collisions are shown in Fig. 9 (π^+ and π^-) , Fig. 10 for kaons, and Fig. 11 for protons and anti-protons. The spectra are derived from data that requires the CC vertex and is thus a measurement of the NSD cross section, but they were normalized to the total INL yield using the corrections factors described earlier. Each spectrum is scaled down by a factor of 10 with increasing rapidity bin. The curves on the figures are the results of the fitting with a Levy (Tsallis) function as discussed later in section III B.

Should the figures show cross sections rather the invariant yields (NSD?), or should be just do that in the spectrum tables at our web pages. Since the web pages may not exists for long, there may be a good reason to include the data as data tables in an appendix? We could show the measured 1/sugmaCC d2ndyppt and give the norm factors to get to the figures

The spectra presented here have not been corrected for feed-down from the weak decays of K^0_s , Λ and higher mass hyperons. The STAR data for mid-rapidity pions

	typical value	systematic uncertainity (%)	From
tracking efficiency (FS)	0.80	4	determined from data
tracking efficiency (MRS)	0.90	4	determined from data and simulations
PID-RICH	0.97	1	data and simulations
Normalization	0.82	10	Vernier scan
Acceptance			
Geant Corrections	0.6-0.85	2	simulations
Trigger Efficiencies	0.99	1	data

TABLE III. Add caption expand to cover all corrections. It also needs to be divided into overall syst, rapidity to rapidity, point-to-point

have been corrected for the contribution from K^0_s decays, this amounts to $\sim$ 12% below 1 GeV/c and $\sim$ 5% ar higher p_T. The main reason for not performing such correction is that the Λ and $\bar{\Lambda}$ yields and their dependence on p_T is not know away from mid-rapidity at 200 GeV where there are measurements by STAR [26] and PHENIX references. In general, the protons from weak decays are found at an average lower p_T than the parent Λ (such shift in $p_T$roughly scales by M_p/M_Λ). Since most weak decays take place before reaching the first tracking detector (either TPM1 or T1) and we apply a fairly wide vertex constraint, most if not all of the protons from the weak decays will be reconstructed and identified as protons. To quantify this further, we have performed detailed simulations of the Λ spectrum with a spectral exponential forms in m_T and several inverse slope parameter values. These simulated data are reconstructed in the complete BRAHMS analysis chain. The resulting proton spectra are integrated to extract the rapidity density yields at different rapidities. From this exercise, we determined that BRAHMS spectrometers do measure 90% of the decay protons in the MRS, and 80% in the FS. Furthermore, these results imply that, for model dN/dy comparisons, one can take a fraction of (0.90 or 0.80 dependent of rapidity) of the 64% of a given lambda yield to compare with data. To compare the p_T dependence of spectra one can add the model proton spectra with a derived decay proton spectrum from lambdas where the p_T scale is scaled by the mass ratio. The analog applies to anti-lambda and anti-proton spectra and yields. This procedure has been applied to the PYTHIA comparisons discussed later in this paper.

Thus the integral of the yields closely matches the sum of direct proton spectra and those of decay protons from hyperons. It was also studied in details for Au+Au reactions at 200 GeV [19, 27]. In those reactions the K/π and Λ/p ratios are higher, 0.2 and 0.9 respectively, than expected for the $p+p$ reactions presented here. The expected ratio Λ/p is ≈ 0.4 at 62.4 GeV and the $\bar{\Lambda}/\bar{p}$ 0.4[28]. We have estimated the contribution to the pion spectra from weak decays to be less than 2% and no correction was applied.

1. Particle Ratios

The ratios of like particle spectra measured in 200 GeV $p+p$ collisions, at selected rapidities, are shown in the 4 left columns of Fig. 12. The ratios have been extracted by taking the ratios of spectra extracted in one field polarity vs the negative yields from an opposite polarity; this reduces the systematic errors. The pion ratios have constant values near 1 at mid-rapidity and show a strong p_t dependence at the highest rapidity. The kaon ratios appear constant near mid-rapidity and decrease with rapidity. A strong p_t dependence is seen at high rapidity. In similar fashion, the ratio for protons shows a more or less constant behavior with values near 0.8 at mid-rapidity which then decrease strongly with rapidity.

The like particle ratios for the 62.4 GeV data are shown in the 2 right-most columns of Fig. 12. As was the case for the 200 GeV data, the pion ratios have values close to 1 at mid-rapidity. and decrease fast at forward rapidities. The kaons show a similar behavior. Within the statistics of our measurements we do not observe a p_T dependence of the ratios up to p_T=2 GeV/c. The p_T averaged value are $\pi^-/\pi^- = 0.97\pm$ 0.015 (stat) $\pm0.03(syst)$, $K^-/K^- =$ $0.74\pm$ 0.024 (stat) $\pm0.04(syst)$, and $p/\bar{p} = 0.50\pm$ 0.03 (stat) $\pm0.04(syst)$. At $y \sim 3$, the small $\bar{p}$ yield produces a very small value of $\bar{p}/p$.

Figure 13 shows the ratios of p/π^+ and $\bar{p}/\pi^-$ for the data at 62.4 and 200 GeV for different rapidity bins. The behavior of the 200 GeV ratios as function of p_T does not change much for small shifts in rapidity, but shows strong variations when going from y 0 to y 3 specially for the negative ratio. The right panels of Fig. 13 shows the ratios extracted from the 62.4 GeV events. The increase in value for these ratios as function of rapidity is much

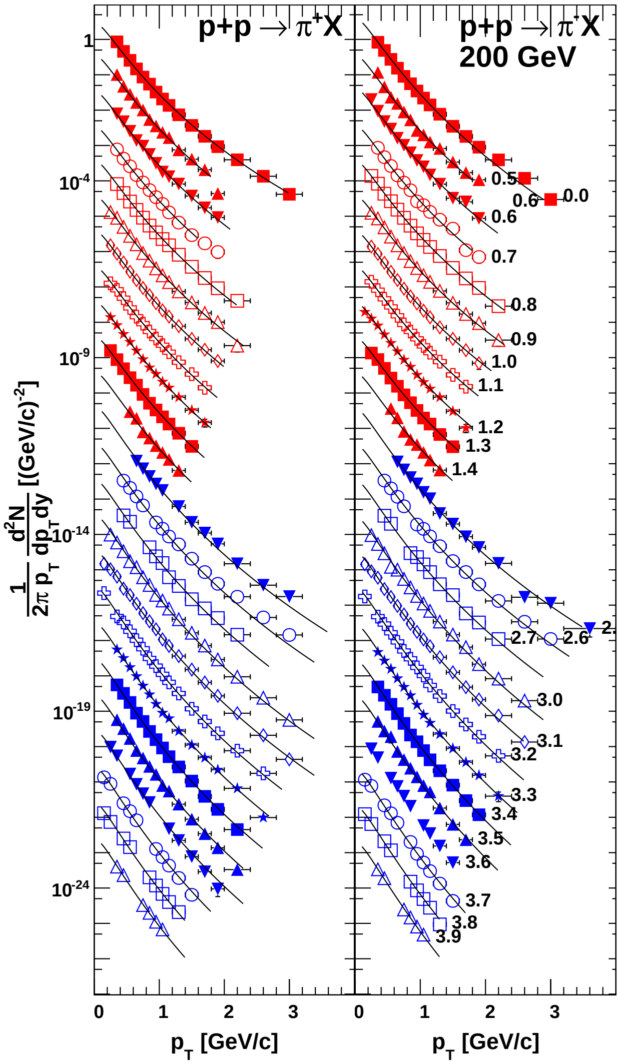

FIG. 9. (Color online) 200 GeV invariant transverse p_{T}spectra for π^+ and π^- for rapidities as indicated in the figure. The spectra for each rapidity bin is scaled down by a factor of 10 from the previous.The curve are result from fits to the spectra with the Levy function as described in the text.

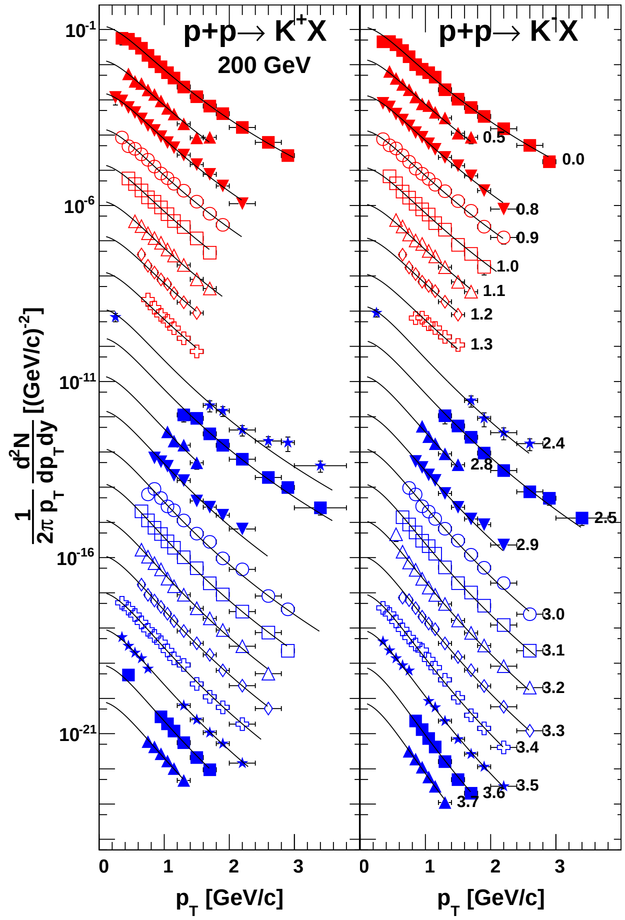

FIG. 10. (Color online) 200 GeV invariant transverse p_{T} spectra for K^+ and K^- for rapidities as indicated in the figure. The spectra for each rapidity bin is scaled down by a factor of 10 from the previous.The curve are result from fits to the spectra with the Levy function as described in the text.

stronger than the one found at 200 GeV. This rapidity and energy variation of these ratios has been discussed in detail in a longer paper which includes Au+Au data [29].

Figure 14 shows the K^+/π^+ ratios (top panels) and the K^-/π^- ratios (bottom panels) for the 200 (left panels) and 62.4 collisions (right panels) at several values of rapidity indicated in the legends. A slight decrease on the value of the K^+/π^+ ratios with increasing rapidity is seen at both energies. A much stronger decrease with rapidity has been measured in the K^-/π^- ratios. That variation is much stronger at the lower energy (62.4 GeV).

2. Comparison to ISR data

Proton+proton collisions were studied extensively in collider mode at the CERN ISR at energies ranging from $\sqrt{s}$= 29 to 62.4 GeV. Of particular relevance for this work are the results from several experiments at 62.4 GeV. The BRAHMS dataset has in general much better statistics than the older ones. It is though still important to check consistency between the datasets. For the mid-rapidity data we compare our pion measurements with those of Alper [30] and Guettler [31] in the upper panel of Fig. 15. The data of Guettler extend to lower p_{T} than the present data, and it shows a turnover of the cross section, which is consistent with a thermal description of the spectrum (exponential in m_T or Boltzmann distribution). This demonstrates that the assumption of a power-law spectrum often used by the heavy ion community is not justified, and that a description using the Levy function as discussed in the next section takes this low-p_{T} feature into account. The data of Alper et al.

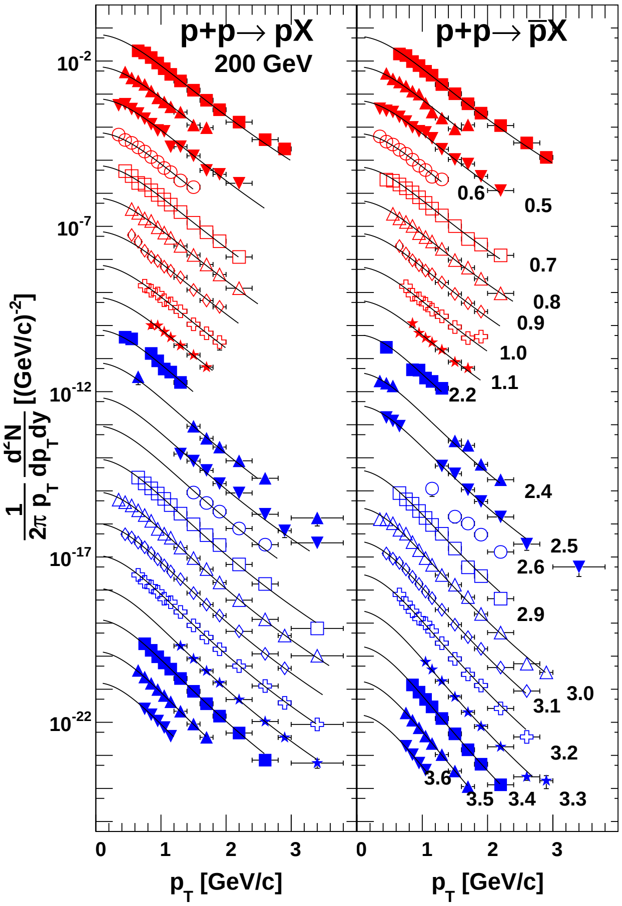

FIG. 11. (Color online) 200 GeV invariant transverse $p_T$spectra for proton and $\bar{p}$ for rapidities as indicated in the figure. The spectra for each rapidity bin is scaled down by a factor of 10 from the previous.The curve are result from fits to the spectra with the Levy function as described in the text.

are in good agreement with ours, while those of Banner are somewhat higher by about 20-30% for the p_T-range of 0.5-1.5 GeV/c.

In the lower panel of Fig.15 we compare our proton and anti-proton data with those of several ISR experiments [32–34]. The agreement for protons is quite good. For the $\bar{p}$-data the older data in general are clearly above the present data. These data do also give rise to ratios of $\bar{p}$/p above 1, which is clearly not reasonable, and do not consider the disagreement an issue.

Fewer data exists at forward rapidity at 62.4 GeV. Cross section of π^- were measured vs. x_F by Albrow [36] at energies up to 52.4 GeV at a fixed angle relative to beam rapidity. Our data has a small region of overlap i.e. rapidity 3.4 and $x_F \sim 0.3$ where the data agrees well with this systematic within $\sim$ 10%. We have also compared our data at mid-rapidity with recently published PHENIX data on 64.2 and 200 GeV $p+p$ collisions[35]. We find that the agreement at 62.4 GeV is overall very good within the statistical errors quoted by each experiment.

3. *Comparison to other 200 GeV $p+p$ RHIC data*

As mentioned before both STAR and PHENIX have published data at 200 GeV one more for PHENIX[35, 37] at mid-rapidity. The STAR data are normalized to the Non Single Diffractive) NSD cross section. We have the data in the p_T-range of 0.2 to 2.0 GeV/c and the overall agreement is within 10-15%. Taking into account that the STAR pion data are corrected for weak decays our pion distributions may be about 10% higher than STAR in the low p_T-region. The PHENIX data are normalized in a similar fashion as our data to the Inelastic INL cross section of 42 mb. Comparing the pion and kaon spectra we find that our data are about 25% higher than PHENIX, but with a similar p_T-dependence. Since the systematic error on the respective Vernier scanned cross section are 8% for PHENIX and 15% for us, these results are not quite compatible. As an additional cross check on this we compared the measured $dN/d\eta$ from UA5[38] and PHOBOS[39] with the dN/dy for pions as measured by PHENIX and BRAHMS. By studying the results of PYTHIAcalculation using several different tunes we observe that the ratio $dN/dy(\pi^+)/dNd\eta$ is ≈ 0.5. The INL $dN/d\eta$ at y=0 is 2.2 thus the predicted pion multiplicity should be 1.1. We measure 1.25 and PHENIX 0.82-0.92 depending on the extrapolation, so it is tempting to conclude that there is a systematic difference between BRAHMS and PHENIX, most likely the two results being respectively too high and too low compared to other measurements. Including the STAR results in this comparison supports this notion. As said earlier we tabulate our results for 200 GeV normalized to the NSD to exclude the systematic error on the σ_{CC} in our measurements.

B. Rapidity Distributions

Since the p_T-spectra do not cover the entire p_T range we have to extrapolate the spectrum towards lower and higher p_T (less important) to extract the rapidity densities. Different functional forms has been proposed and used over time. Fairly recently the Levy functional form [40–42] has been used for relativistic heavy ion reactions since it combines the feature of a power-law behavior at high-p_T with that of a exponential in m_T at low p_T. In particular for pions do the extrapolation play an important role due to the low average p_T of about 300-400 MeV/c and our coverage that only for selected rapidities extends down to 200 MeV/c. The functional form of the invariant distribution is

$$\frac{1}{2\pi p_T}\frac{d^2N}{dydp_T} = \frac{1}{2\pi}\frac{dN}{dy}\frac{(n-1)(n-2)}{nT(nT+m_0(n-2))} \times \left(1+\frac{(m_T-m_0)}{nT}\right)^{-n} \quad (3)$$

which we use to analyze the 200 GeV data. To minimize the effect of different p_T coverage versus rapidity we performed a global fit to extract yields. The parameters

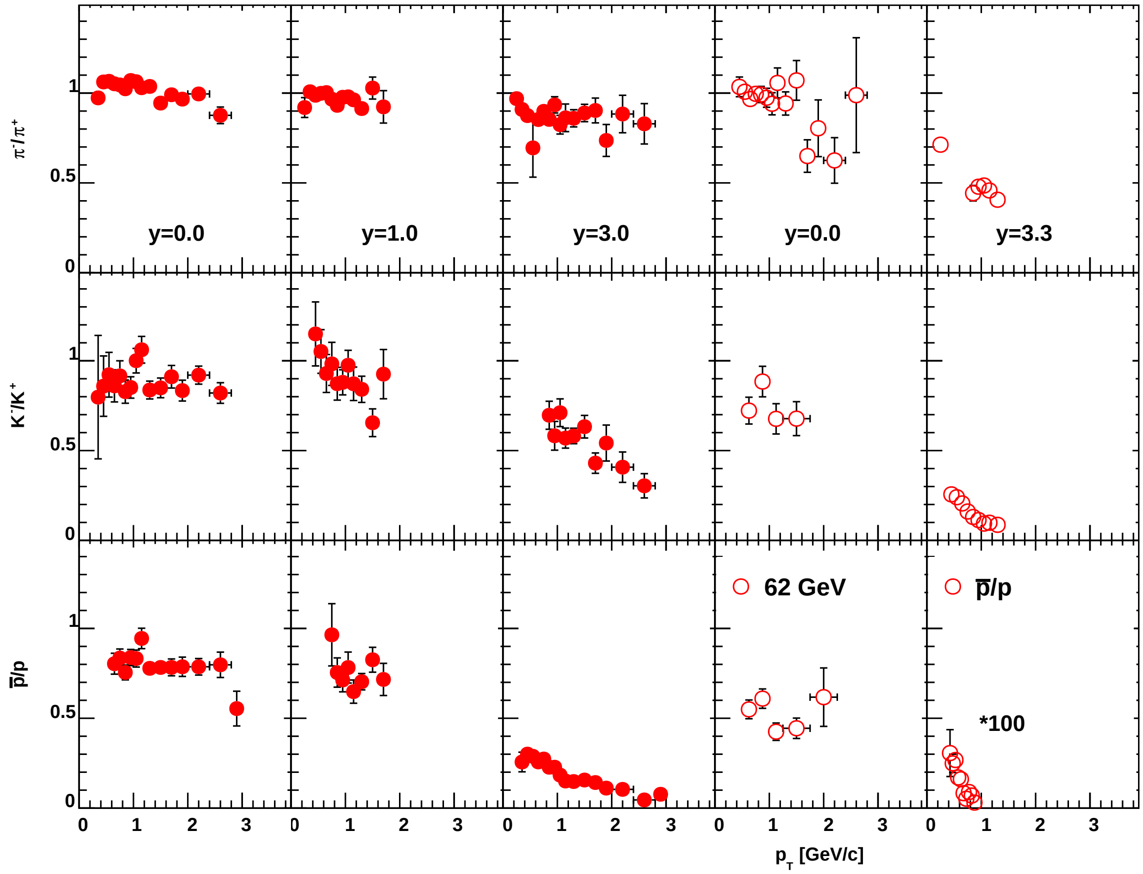

FIG. 12. (Color online) Negative to positive particle ratios for pions, kaons, protons at 200 GeV (left 4 columns) and 62.4 GeV (right 3 columns).We should redo the analysis at y 0 by taking ratios of A/B polarities and then averaging to reduce systematic errors. We should also remove the outliers

in the Levy function (n, T) are assumed to be slowly varying functions of rapidity, ie $T = T_0 + a_1 y + a_2 y^2$ and $n = n_0 + b_1 y + b_2 y^2$. we use the form with m_T -m as the independent variables. The Tlassis functional form actually uses m_T, the functional form is identical if the T is replaced by $T.(1 + m_0/nT)$.

Such a fit reduces the systematic variation otherwise present in the parameters due to varying $p_{\rm T}$ coverage at different rapidities and to systematics from combining settings, but at the expense of a higher χ^2 for each setting. In the fitting procedure we add in quadrature a 7% error representing the point to point systematic error estimate. For the 200 GeV data we present the results of such fits compared to the data in the spectral figures.

At 62.4 GeV we do not make a global fit including all rapidity bins at once, since at the most forward angle the spectral shape is very much influenced by the kinematic limit. Rather the data set is divided into two groups around mid-rapidity and the forward settings where combined fits are then done. The 62.4 GeV data have much fewer data points, and less coverage in y-$p_{\rm T}$ so extraction of dN/dy is restricted to much fewer points. The experimental data taking was optimized to get good coverage for protons, thus having limited coverage in particular for kaons.

The extracted rapidity densities dN/dy are shown in Fig. 16 for 200 GeV in the left panels, for pions, kaons and protons. Positive particles are represented by the closed symbols and anti-particle are shown together represented by the open symbols. We see in general a flat distribution to $y \sim 1$ and then a decrease at the higher rapidities for all particles except protons which show an increase above $y \sim 2$ for both energies.

The right panels of Fig. 16 show the 62.4 GeV rapidity densities. The 62.4 GeV data are in general lower than the 200 GeV data. The pions show the same sort of behavior as the 200 GeV data, namely a flat distribution to $y \sim 1$ and then a decrease. The protons, in contrast, show a much stronger increase at the forward rapidities than the 200 GeV data. That is a consequence of the proximity to the beam rapidity. The anti-protons show a much stronger decrease.

Using the parameters extracted from the fits, we can derive the average transverse momentum, $\langle p_T \rangle$ for each of the particle species. This is shown in Fig. 17. In the left panel where we show the data for $\sqrt{s} = 200$ GeV, the dashed lines represent the $\langle p_T \rangle$ derived from the parameters when the global fits were performed. The symbols

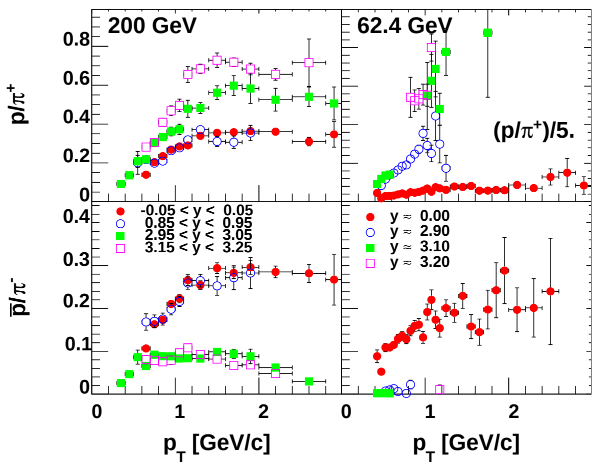

FIG. 13. (Color online) Particle ratio of protons over pions for p/π^+ (upper panels) and $\bar{p}/\pi^-$ (lower panels) for rapidities indicated by the legend. Data from 200 GeV are in the left panels, the 62.4 GeV data in the right.

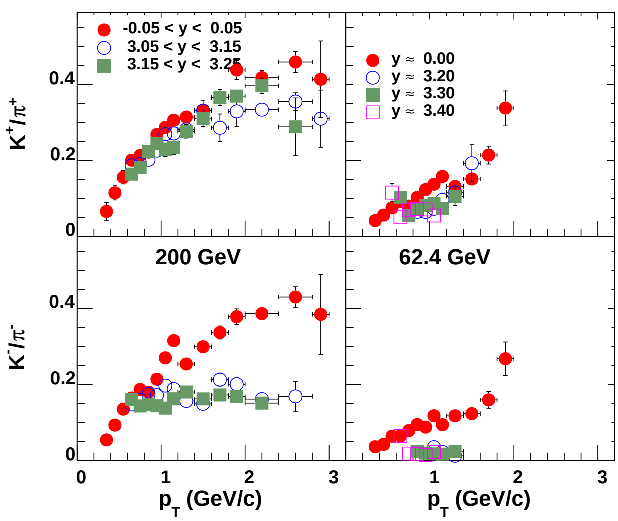

FIG. 14. (Color online) Particle ratio of Kaons over pions for K^+/π^+ (upper panels) and K^-/π^- (lower panels) for rapidities indicated by the legend.Data from 200 GeV are in the left panels, the 62.4 GeV data in the right. Make the figure taller, change symbol layout open/closed for b/w -KH

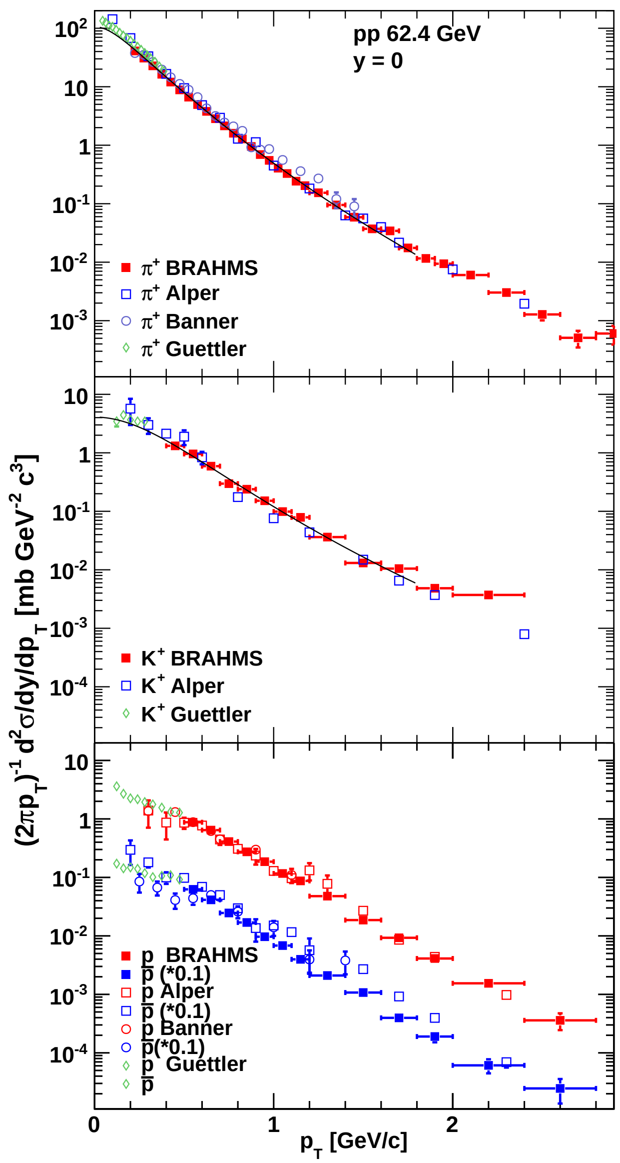

FIG. 15. (Color online) Comparison of ISR data with present 62.4 GeV data at mid-rapidity. The top panel is for π^+, the middle if for K^+ and the bottom panel for protons and $\bar{\mathrm{p}}$. The $\bar{\mathrm{p}}$ cross sections have been divided by a factor of 10 for clarity. Make the plot taller and legend text bigger- FV

show the values of $\langle p_T \rangle$ extracted when individual fits are performed on rapidity bins that have coverage below $\langle p_T \rangle$. We note that these two quantities agree in general.NOTE the figure = fits must be updated to to show this- it is worthwhile to do IMHO

The magnitude of $\langle p_T \rangle$ for the 62.4 and 200 GeV data are similar for all particle species shown.

1. *Longitudinal Scaling*

It was conjectured by Beneke et. al [43] that particle production near beam rapidity should be independent of beam energy when cross sections are measured relative to the beam rapidity i.e. vs. the variable $y - y_{beam}$. In most work the dependence of the rapidity densities dN/dy or pseudo-rapidity $dN/d\eta$ has been explored. The original expectation is this this should also hold for differential cross sections i.e. $\frac{d^2N}{dp_t dy}(y - y_{beam}, p_t)$.

This was for instance demonstrated in the survey of ISR data for the energy range 26-52 GeV in the paper

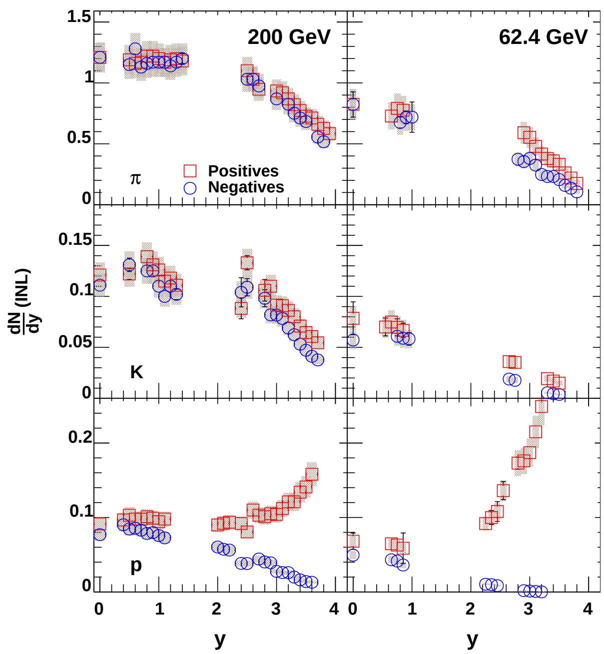

FIG. 16. (Color online) Invariant rapidity densities for pions, kaons and protons at 200 GeV and 62.4 GeV. Open squares represent the positive particles and open circles represent the negative particles. The solid curves represent the positive particle predictions of PYTHIA tune 320 and the dashed curves represent the negative particle predictions of PYTHIA. This should be moved to a later figure, and not done here

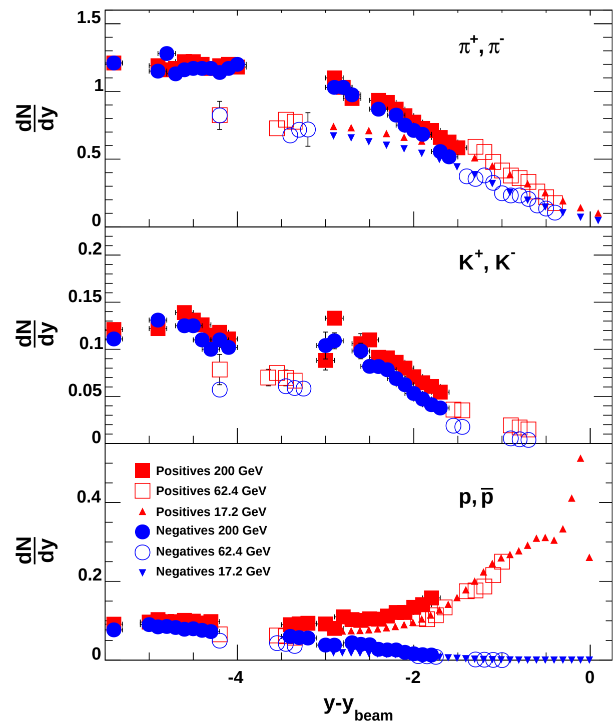

FIG. 18. (Color online) π^+, π^-, K$^+$, K$^-$, p and $\bar{p}$ for 62.4, 200 GeV. The data are plotted to illustrate the longitudinal scaling

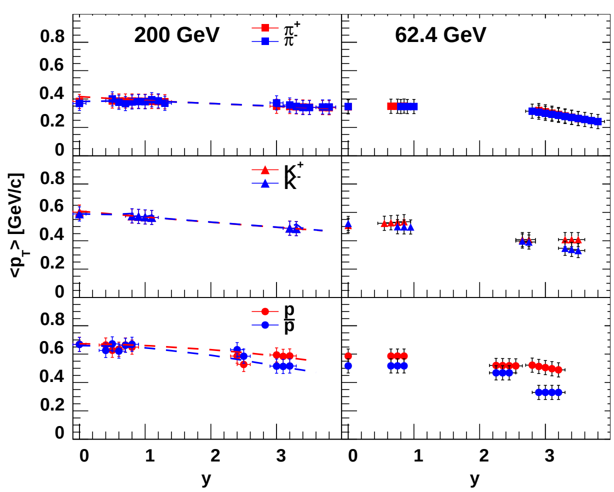

FIG. 17. (Color online) $\langle p_T \rangle$for pions, kaons, protons and anti-protons from 200 GeV (left) and 62.4 GeV (right).

by Capiletti. This longitudinal scaling has also been observed in cosmic ray data and in AA collisions (see (Otterlund) and (Busza) end references therein. Here we explore such scaling in our $p+p$ data at 62.4 and 200 GeV.

In Fig. 18 we show the same distributions as shown in Fig. 16, but consolidated and plotted vs the difference in rapidity from the beam rapidity, $y - y_{beam}$. The top panel shows the π^+ and π^- dN/dy and the bottom shows the same for $p, \bar{p}$. We show our data from 62.4 and 200 GeV as well as pion and proton data from NA49 [44, 45] with $\sqrt{s} = 17.2$ GeV. We note that in the region of overlap of all energies that the data are consistent for rapidities near the beam rapidity of the respective system. This would suggest that particle production near the beam rapidity is governed by the distance from the beam rapidity regardless of the energy. This appears to be consistent for $17.2 < \sqrt{s} < 200$ GeV.

Figure 19 shows the net proton distributions plotted vs $y - y_{beam}$. These are derived from the difference of the proton and anti-proton distributions in Fig.16. There is an overlap in the net-proton dN/dy for all data where there is an overlap in rapidity. This will be discussed further in the next section where this information is transformed into information on net-baryon distributions.

2. *Stopping*

Stopping in heavy ion collisions has been of significant interest for a long time interest [46–48] We have extended our study of stopping to the $p+p$ system at 200 and 62.4 GeV using the present data.

In order to study stopping, it is necessary to obtain the net baryon dN/dy distributions. Unfortunately, we

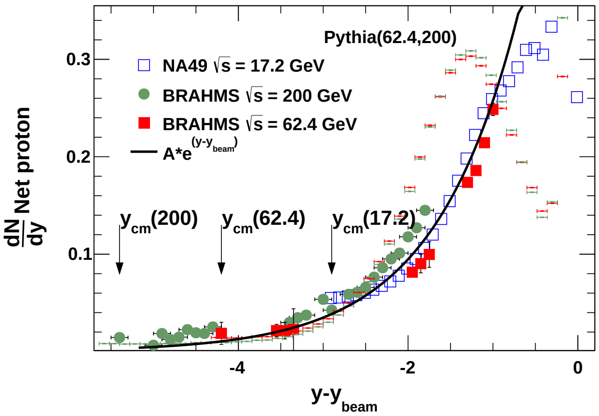

FIG. 19. (Color online) Net-protons from 62.4, 200 GeV and 17.4 GeV (NA49). The data are plotted to illustrate the longitudinal scaling. The three arrows starting from the left represent mid-rapidity for 200, 62.4 and 17.4 GeV $p+p$ systems, respectively.

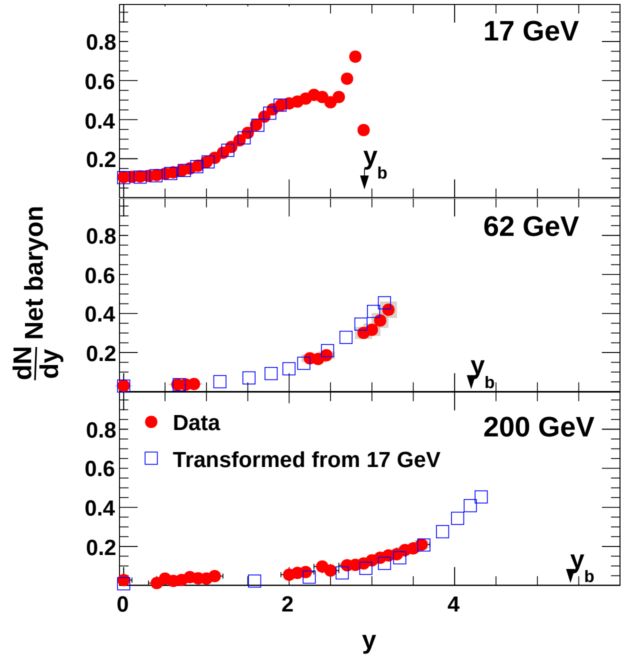

FIG. 20. (Color online) Net-baryon dN/dy distribution for 62.4 GeV (center panel) and 200 GeV (bottom panel). The data are indicated by the solid points and the predictions of the PYTHIAcalculation are shown by the solid curves. The net-baryon dN/dy distribution derived from the 17 GeV $p,\bar{p}$ [45] is shown in the top panel. The open squares show the net-baryon dN/dx_{F} at 17 GeV transformed to dN/dy at the respective energies.

only measure protons, so the closest direct measurement that we can make is net-proton dN/d$\dot{y}$The net proton dN/dy has already been shown in a longitudinal scaling context in section VI.D. In order to obtain the net-baryon dN/dy from what we measure, the net-proton dN/dy , it is necessary to correct according to:

$$\frac{dN_{B-\bar{B}}}{dy} = \frac{dN_{p-\bar{p},meas}}{dy}\frac{n_p+n_n+n_\Lambda}{n_p+c_1 n_\Lambda} \tag{4}$$

where $\frac{dN_{p-\bar{p},meas}}{dy}$ is the number of measured net protons, n_p is the number of true net protons, n_n is the number of net neutrons and n_Λ is the number of net Λ. c_1 is the number of protons from weak decays for each Λ, found to be 0.53 ± 0.05 using monte-carlo simulations [47].

The correction factor in Eq. 4 can be rewritten as

$$\frac{1+\frac{n_n}{n_p}+\frac{n_\Lambda}{n_p}}{1+c_1\frac{n_\Lambda}{n_p}} \tag{5}$$

indicating that the important parameters are the net neutron to net proton ratio, n_n/n_p, and the net lambda to net proton ratio, n_Λ/n_p. We used PYTHIAto estimate n_n/n_p and n_Λ/n_p as a function of rapidity for $\sqrt{s}$ = 17, 62.4 and 200 GeV. To constrain PYTHIA, we combined the Lambda dN/dy at measured by STAR [26] at $\sqrt{s}$ = 200 GeV at mid-rapidity combined with our proton measurement at mid-rapidity to obtain a value of $n_\Lambda/n_p = 0.2575 \pm 0.106$. The results agree within errors. We therefore made fits to the PYTHIA predictions of n_n/n_p and n_Λ/n_p as a function of rapidity for each energy and used that to generate a correction factor function for each energy. The corrections that we make therefore assume that PYTHIA predicts both the rapidity and energy dependence of n_n/n_p and n_Λ/n_p and the only point tied to experimental data is n_Λ/n_p at mid-rapidity at $\sqrt{s}$= 200 GeV.

Using these factors in Eq. 5 and calculating $\frac{dN_{B-\bar{B}}}{dy}$, we obtain the net-baryon rapidity distribution for our data at both RHIC energies shown as solid circles in Fig.20. We also show the net-baryon rapidity distribution that we derive from the NA49 data [45] in the top panel of Fig. 20.

We note that there is a plateau of very small $B-\bar{B}$ at mid rapidity for the 200 and 62.4 GeV data that increases as the beam rapidity is approached. It is also to be noted that the data at 62.4 GeV rises significantly higher than at 200 GeV, a result of the proximity to the beam rapidity of the lower energy. The 17 GeV data [45] are comprised of a complete measurement from mid-rapidity to the beam rapidity.

Stopping is quantified by using the average rapidity loss, $\langle\delta y\rangle = y_p - \langle y\rangle$, where $\langle y\rangle$ is calculated using

$$\langle y\rangle = 2\int_0^{y_p} y\frac{dN_{B-\bar{B}}}{dy}dy \tag{6}$$

In references [47] and [48], the net-baryon distributions were fit to a number of functions that were constrained by baryon conservation. To obtain stopping, the functions with the extracted fit parameters were used in equation 6. It was shown that the results were relatively insensitive to the functional form once the constraints were imposed.

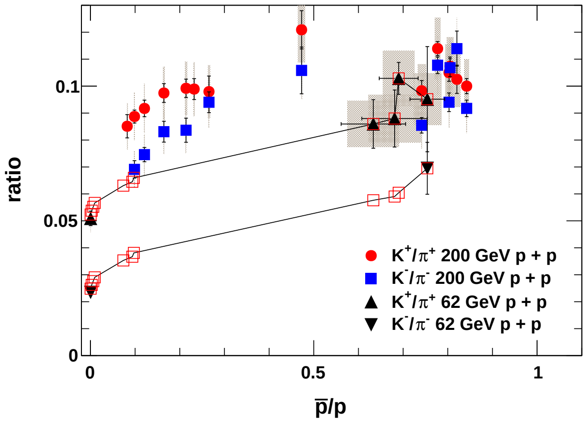

FIG. 21. (Color online) K/π ratios vs $\bar{p}/p$ for 200 GeV and 62.4 GeV.

In this work we exploit the complete distribution that has been measured at 17 GeV [45]. In that paper, proton $dN/dx_{\rm F}$ was quoted as well as dN/dy. We have transformed the proton $dN/dx_{\rm F}$ to dN/dy at 17 GeV. These data are shown as open squares in the top panel of Fig.20 and, indeed, overlap the quoted dN/dy after applying the correction factors. We then transformed the 17 GeV $dN/dx_{\rm F}$ to dN/dy at the RHIC energies and the results are shown as open squares in the 62.4 and 200 GeV panels. We note that the net-baryon dN/dy transformed from the 17 GeV data overlaps well with the measured rapidity range for 62 and 200 GeV. This shows is consistent with the notion that $\langle y \rangle$ does not change much over the energy range from 17 GeV to 200 GeV. Include ref to recent Wolchin paper?

3. Particle Ratios

The closed symbols in Fig.21 we show the integrated values of the K^+/π^+ and K^-/π^- ratios plotted vs the integrated values of $\bar{p}/p$ ratios for 200 and 62.4 GeV in the left and right hand panels, respectively. The $\bar{p}/p$ ratios are related to the baryo-chemical potential and such a correlation might provide information on the dependence of strangeness with baryo-chemical potential. The x axis of $\bar{p}/p$ is qualitatively an inverse rapidity scale. We note that both the K^+/π^+ and K^-/π^- ratios show an increase with $\bar{p}/p$ at both energies. Though there is not a complete overlap in range, the values are consistent with being similar at 62 and 200 GeV

C. Average Multiplicities vs. energy

In Ref. [49] a summary is given of average identified particle multiplicities integrated over all phase space, up to and including ISR energy data. The present data allows us to add information for 4π yields pions,kaons and $\bar{\rm p}$ at $\sqrt{s}$ = 200 and 62.4 GeV. The present data provides measurements of dn/dy up to about rapidity 3.5-4 for charged hadrons. We estimate the 4π yields by two means. Firstby fitting the rapidity distributions to a Gaussian distribution and extracting the yield from the functional integrals. The measurements typically covers 80% of the yield assuming symmetry around $y = 0$. The systematic errors are estimated taking into account the errors from the normalization of mid-rapidity and forward rapidity data respectively. The data are presented in Tab.III C.

specie	62.4 GeV Gaus	Integral	200 GeV Gaus	integral
π^+	4.76±0.16	4.86	9.5±0.2	9.1±0.2
π^-	4.19±0.19	4.00	9.0±0.2	8.7±0.2
K^+	0.37±0.02	0.36	0.94± 0.05	0.87±0.05
K^-	0.25±0.02	0.26	0.79±0.04	0.80±0.05
$\bar{\rm p}$	0.15±0.01	0.15	0.43±0.01	0.44± 0.02

TABLE IV. 4π multiplicities for 62.4 and 200 GeV extracted from the present data. errors need evaluation and systematic estimate too.

In Fig.22 we show the integral yields from the ISR data together with the present 62.4 and 200 GeV data, and those from SPS energies (NA27 [50] and NA49 [44]). The curves in the figure show fits to the data combining the previous low energy data with the present data at 62.4 and 200 GeV. The fit function is given by

$$\langle N \rangle = a + b \ln s + c\sqrt{s} \quad (7)$$

The quality of the fits shows that the present data continues the systematics established with the lower energy data. We also extrapolate the fits to $\sqrt{s}$ = 5.2 TeV to provide a prediction of the multiplicities to be expected at the LHC if the present systematics continue. The parameters extracted in the fits are shown in Table III C. my latex gives the wrong table ref i.e pointing to the section not the table number!. Evaluate error due to extrapolations. Treat protons as 2*pbar+1.6 to account for un-measured beam protons in both directions

We note that the total charged particle multiplicities extracted from our 200 GeV data i.e. the sum of pions, kaons, and protons is $\sim 21.7 \pm 0.6(stat) \pm 2.0(syst)$ in good agreement with the PHOBOS $dN/d\eta$ measurements [39] of 20.2 ± 1.8. The 62.4 GeV 4π-integrals from the present data of identified particles seems lower the overall systematics from ISR. On the other hand in the table we calculate the total charged particle multiplicities over 4π by adding the pions, kaons p-bar and assuming that the total proton multiplicity is equal to the produced prtons

species	a	b	c
π^+	-3.98	2.18	3.64
π^-	-5.00	2.22	4.76
K$^+$	-1.03	0.36	1.10
K$^-$	-0.73	0.26	0.71
$\bar{p}$	-0.76	0.20	1.00

TABLE V. Parameters extracted in the fits to 4π multiplicities vs energy

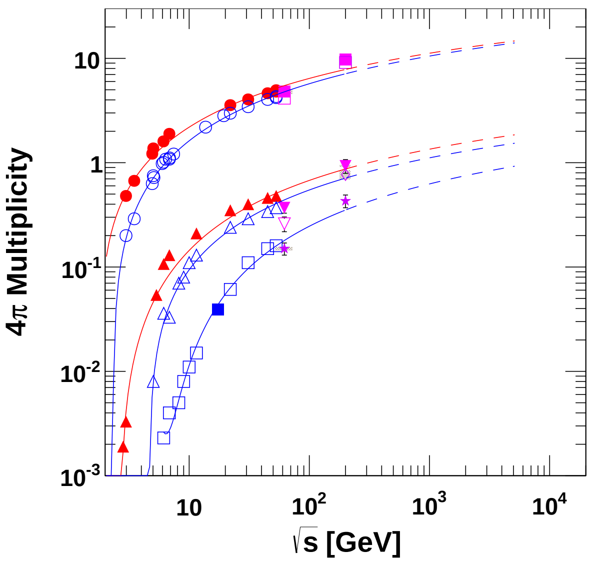

FIG. 22. (Color online) Full phase space average charged particle multiplicity for identified hadrons as function of $\sqrt{s}$. Lower energy data are from Refs. [44, 49, 50].

specie	62.4 GeV RMS	200 GeV RMS
π^+	1.93±0.2	2.40±0.1
π^-	1.78±0.2	2.34±0.2
K^+	1.67± 0.05	2.33±0.2
K^-	1.49±0.04	2.20±0.2
p̄	1.20±0.01	1.90± 0.2

TABLE VI. Extracted RMS for 62.4 and 200 GeV rapidity distributions errors need evaluation and systematic estimate too.

set equal to the anti-protons, and the beam fragmentations i.e. 1.4 per collisions. That multiplicity is 11.7 ± 0.6 in good agreement with the value of 12.26 ± 0.21 for the Inelastic cross section of Ref. [51]. We do though want to point out that the integral 4π values from ISR for identified particles have been derived from measurements at $p_{\rm T}$=0.4 GeV/c assuming a rapidity independent spectra shape of e^{-Bp_T}, which based on our measurements is not warranted up to the beam rapidity $y \sim 4.2$.

IV. COMPARISON TO THEORY

A. Comparison to pQCD

As mentioned in the introduction it has been demonstrated that Next to Leading order (NLO) describe pion and kaon transverse spectra at $p_{\rm T}$higher than ~ 2 GeV/c both at mid-rapidity and at forward rapidities up to $y \sim 4$ at 200 GeV. It is also known that at lower energies ~ 19 GeV NLO pQCD even fails at mid-rapidity, whereas PHENIX [52] has shown that the π^0 transverse spectrum at 62.4 GeV is well described at mid-rapidity. With the available data at 62.4 GeV we will explore the current status of pQCD calculations, and offer the viewpoint that the present forward rapidity data are useful in further constraining the fragmentation functions.

In a previous publication [7] we compared π, K and p data at 200 GeV with pQD calculations at y=2.95 and 3.3. These calculations were performed with the mKPP fragmentation functions (FF). These were not truly flavor separated, but applied a simple ansatz for the favored to non- favored quarks ratios. Since then a new global fit has been performed by Florian, Sasso and Stratman [53] that incorporates $e^+ - e^-$, HERA as well as $p+p$ data from RHIC in the determination of flavor separated FFs. Here we will compare our data at both energies with calculations that utilizes these newer FFs. In Fig. 23 we compare $p_{\rm T}$-spectra with the NLO pQCD calculations for identified hadrons at 3 selected rapidities for 200 GeV.

In the leftmost panels, we show the π^+ and π^- , in the middle the K^+ and K^-, and in the rightmost panel the p and p̄. Three selected rapidities go from high in the top row to mid-rapidity in the lowest row. This layout is used in several subsequent figures for the 62.4 GeV pQCD comparison, and in the next section for the comparisons to PYTHIA. In short the calculations are evaluated at equal factorization and renormalization scale $\mu = \mu_F = \mu_R = p_T$ using the CTEQ6M Parton Distribution Functions (PDFs) and the DSS fragmentation functions. Why does the agreement look worse than our old p+p paper, and the DSS fragmentation determination paper. Should be explored by using a linear comparison, or possibly a chi**2 comparison.We have compared this newest analysis with the RD paper and it is quit good - redo this The agreement for $\pi^\pm$ and K$^\pm$ is good at all rapidities. This is not surprising since the previously mentioned BRAHMS data at high rapidities were included in the determination of the DSS FFs. The selected rapidities shown here are slightly different than those in ref [7]. As observed before the proton and anti-proton spectra are reasonable described both in magnitude and slope, whereas at the high rapidity the pQCD do not describe that the anti-proton are much suppressed compared to the protons. This is most likely due to the dominance to

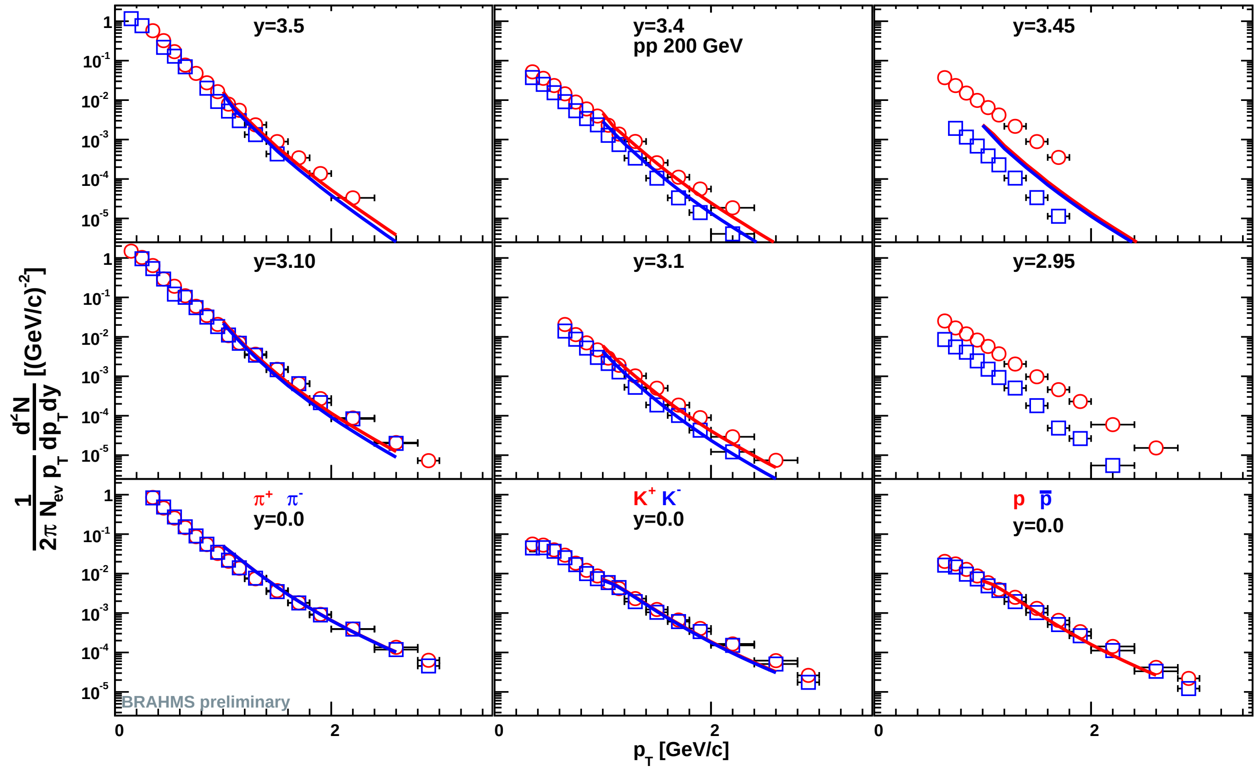

FIG. 23. (Color online) Invariant transverse spectra for π^+, K^+, K^-, p and $\bar{\text{p}}$ at y=0 and at two high rapidities as indicated in the figure compared to NLL pQCD calculations. For kaons and protons the positive particle is indicated by the square (red) points and by the open circle (Blue) for the negatives. The data are from 200 GeV $p+p$.

sea-quarks in the near fragmentation region.

At lower energies it is known that higher order contributions are important, and in particular at the higher rapidities. We have had performed both NLO and Next to Leading Log (NLL) calculations for the 62.4 GeV data. Before we show full comparison we will discuss some features of the NLO and NNL calculations. In Fig.24 we show $\pi^+ p_{\mathrm{T}}$ spectrum at y=3.3 together with the NLO and NLL calculations. As expected the NLL is somewhat higher that the NLO. In the lower panel we show the scale dependence for the NLL calculation by comparing the $\mu = 1$ and the $\mu = 2.0$. It is not shown, but the scale dependence for the LO is about 30% larger. Overall the NLL calculations gives a reasonable albeit not perfect description for the π^+ cross sections.

In Fig. 25 we show similar to the 200 GeV the overall comparisons. Again at mid-rapidity the agreement is quit good. A forward the rapidities the π^+ and K^+ spectra are in good agreement, including the description of the increased steepness of the spectra going from y=2.7 to 3.3 for π^+ and from 3.1 to 3.3 for K^+. There may be a trend towards underestimating the data at the highest p_{T}values. On the other hand both the $\pi^-$and K^- are wastly overpredicted. These are of course the un-favored flavor, and also the FF at these large z values are not well constrained by the data included int the DSS global fits. Inclusion of these data may provide value new information to the overall picture of FF. In addition conclude the in the p_{T}-range of 1-1.5 GeV/c the calculation reproduces the data for π^- and π^+ within 20% thus making the use of perturbative description in the transverse spin asymmetries justified as described in ref [11].

This fairly good agreement between data and NLL calculations may at first glance this is in disagreement with the conclusions of Ref. [54] which indicates that pQCD fails badly at the ISR energies at high x_F. For the 3° data compared in that paper the calculation under-predicts the data by up to an order of magnitude, but this is at larger x_F than we have data for here.

We have investigated the data of Owens [55] as given in the Durham HEP data repository further. The data are given for 4 angle settings in the forward region with mean angles of $\Theta = 3,\ 5,\ 7.5$ and 10 degrees. We observe that the p_T distribution in each setting has the same dependence for each setting, but stops at the kinematic limit. This kind of behavior is not expected since meson production is usual suppressed near the kinematic limit. This is e.g. seen in the data of Ref. [36] that for a fixed angle at 53 GeV show that the cross section start falling rapidly within 20% of the kinematic limit. We therefore are cautious to put to much weight on the data of [55]. We speculate that it is possible that the data have prob-

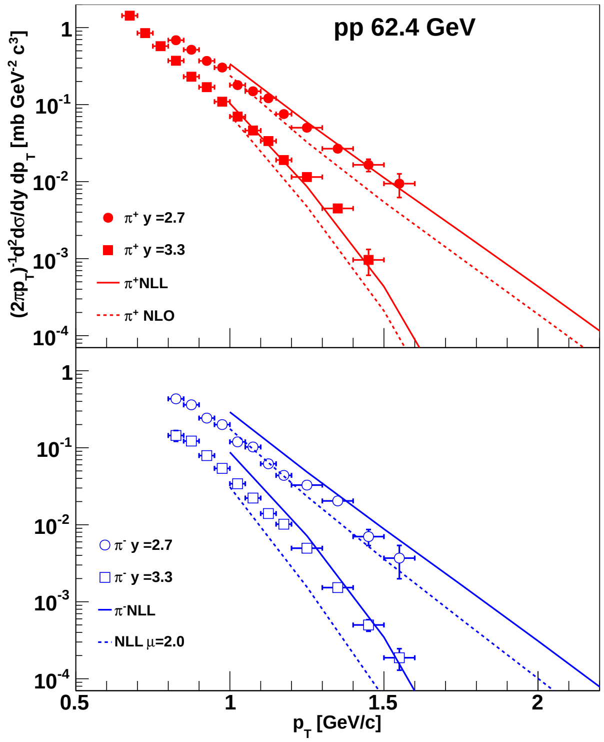

FIG. 24. (Color online) Invariant transverse spectra for π^- and π^+ at 2.7 and 3.3 compared with NLL pQCD calculations as described in the text. Replace with figs comparing pQCD and NLL scale diff for say π^+ only in two panels.

lems e.g. because the π^0 spectra are deduced from the inclusive photons spectrum, that the angular resolution of the detector is so large that the rapidly changing cross section with angle is not taken properly into account.

B. Comparison to Pythia

In addition to describing transverse spectra with pQCD calculations models like PYTHIA [14] are often used to describe $p+p$ collisions. PYTHIA is aimed at describing high-momentum transfer parton processes, but includes a description of soft processes both for the purpose of minimum bias cross section, and as the underlying event (UE) for the hard processes. Recently the development of PYTHIA6 has ceased, and new tunes development are solely done in the framework of PYTHIA8.We therefore have decided to compare the present data to such calculation exclusively.

The parameters for soft processes have in many cases been determined by tuning to underlying events until recently using LEP and Tevatron data, but many of the new LHC results are most relevant for confirming or modifying tunes. So far a number of RHIC data at mid-rapidity and high p_T have been included in the tuning process.

Here we compare selected minimum-bias (Inelastic) results of the present data with PYTHIA (version 8.175) calculations, and present some observations on a subset of the available tunes.

```
what to look at
i) dndy
ii) pi,K,p at y~0
iii) pi, p at high rap
iv) p/pi at low and high rap
comments on non choice of parameters
    i.e. no tune for these


Overall discussion of tunes
200 GeV
tune    pion

100     too soft (data/calc increase at pt~3)
103(Dw) shape good    y~3.7  (slightl  low 0.60 shape ok

201  too soft

300
```

Since the transverse momenta spectra and rapidity density distributions data are normalized to the total inelastic cross section we include the Single and Double Diffractive (SD/DD) processes in addition to the Non Single Diffractive (NSD) processes in the calculations, but not the elastic processes. In Fig.26 we show a selection of transverse momenta spectra, at mid-rapidity

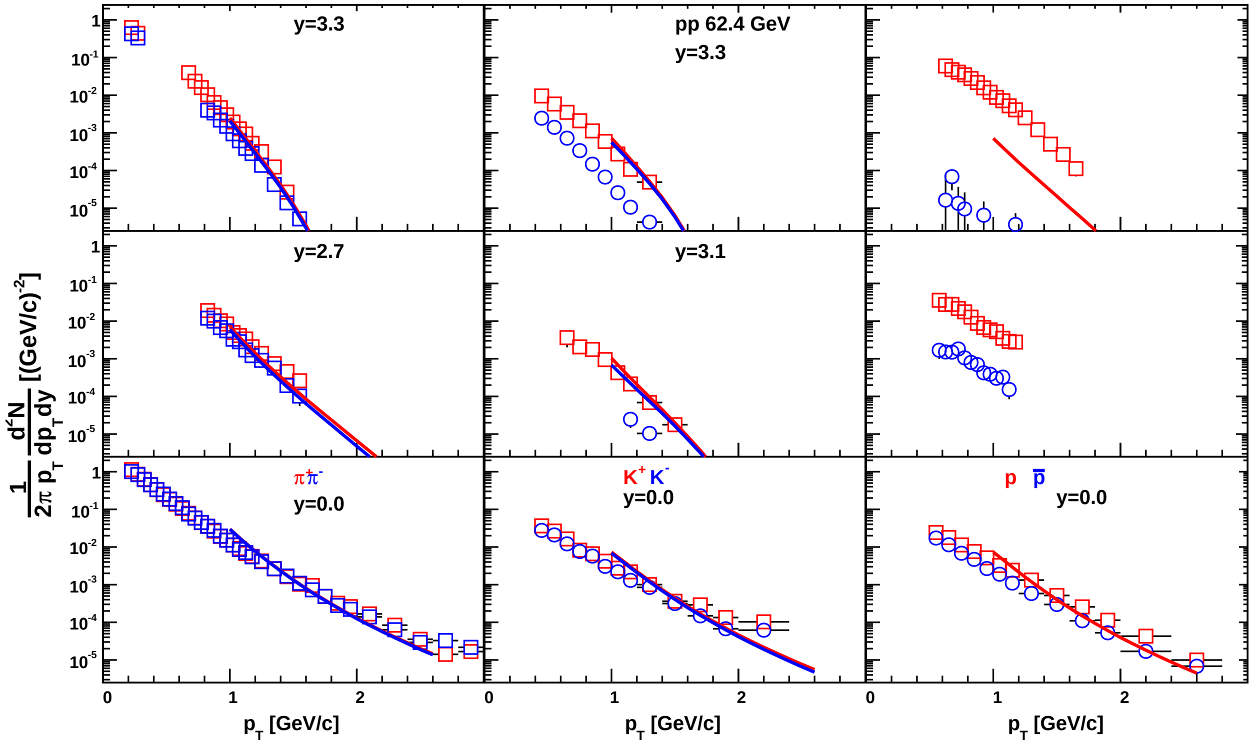

FIG. 25. (Color online) Invariant transverse spectra for π^+, K^+, K^-, p and $\bar{\text{p}}$ at y=0 and at two high rapidities as indicated in the figure compared to NLL pQCD calculations. For kaons and protons the positive particle is indicated by the square (red) points and by the open circle (Blue) for the negatives. The data are from 62.4 GeV $p+p$.

and at two forward rapidities for 200 GeV , the same selections used for the comparisons with the pQCD calculations previously. The results is shown for the Rick Field tune DW (pytune 103). This tune describes Tevatron and mid-rapidity RHIC high-p_{T} data quite well, and the over description of pion and kaon spectra is fairly reasonable at both forward and mid-rapidity.

Repeat the figure of dN/dy just for positives, and with one or two Pythia tunes. Or the Net-dn/dy protons vs energy...

The solid and dashed curves show the predictions of PYTHIA tune 320 [14]. We note a qualitative agreement for all particles at both energies. There is, however, rough quantitative agreement only for pions at $\sqrt{s_{NN}} = 200$ GeV.

The most glaring discrepancy in both the default tunes, but also for other is for the production of proton and antiprotons, not giving the proper distributions of net-protons. It seems that the production of soft net-protons (baryons) do not follow the systematics of data available now at 62.4 and 200 GeV. It may well point to a different mixture between soft and hard processes.

Refer back to net-p.. The solid curves in figure 20 show the $B-\bar{b}$ prediction of PYTHIA for the two RHIC energies as well as the NA49 measurement. The model is in qualitative agreement with the data showing the low net baryon yield at mid rapidity and the bulk of the yield at the higher rapidities for the RHIC data. PYTHIA , however, predicts a faster increase with rapidity than the data shows. The PYTHIAcalculation at 17 GeV exhibits a trend somewhat different than the data starting higher at mid-rapidity and peaking at much lower rapidity.

I think we should add dn/dy say for positives, and show two or 3 different PYTHIA tunes compared to data - including the norm error on the dndy (15-18% on 200 GeV 15 %on 62.4 GeV. we should also reference the HERA analysis of forward protons and neutrons that also point to similar (non flat dn/dx) for proton production- not published from HERA/LHC workshop contribution

To quantify the comparison of the rapidity distribution we compare in Table.IV B the extracted RMS from the 62.4 and 200 GeV data

V. SUMMARY AND CONCLUSIONS

The BRAHMS experiment at RHIC has performed measurements of hadrons in $p+p$ collisions at $\sqrt{s} = 62.4$ and 200 GeV over the widest, most complete range of rapidity to date and in the low p_{T}-region. From measure-

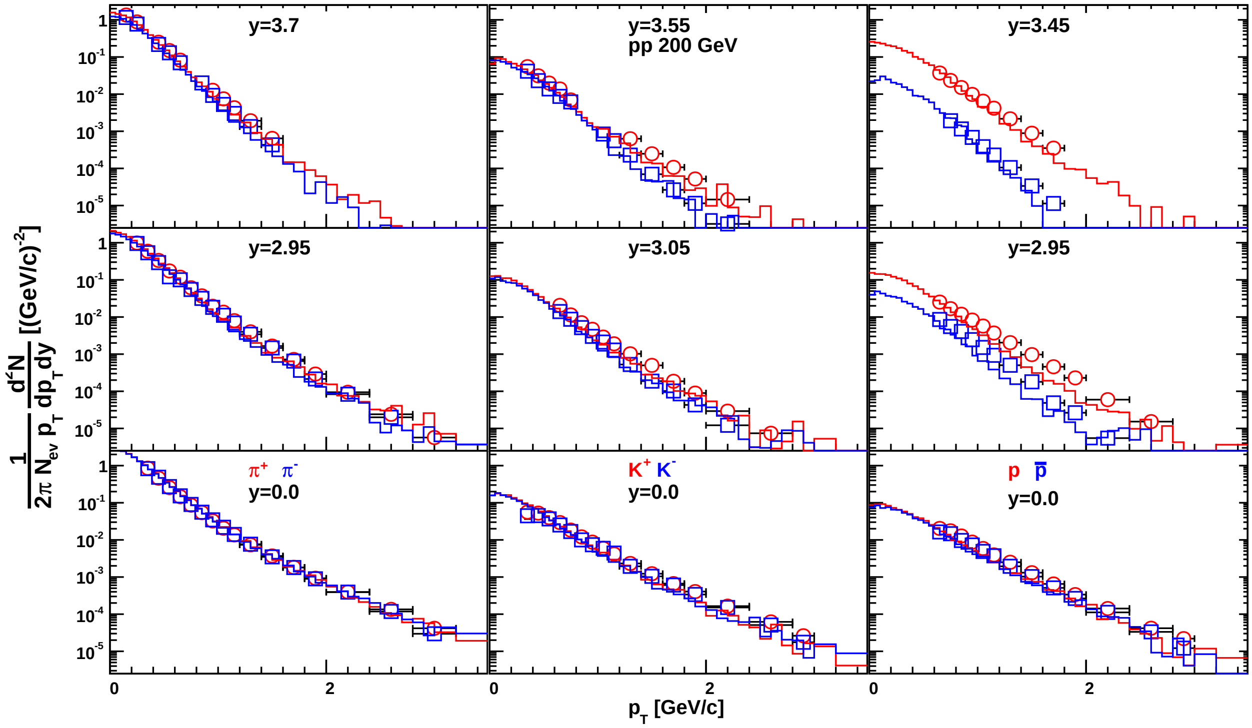

FIG. 26. (Color online) Invariant transverse spectra for π^+, K^+, K^-, p and $\bar{\text{p}}$ at y=0 and at two high rapidities as indicated in the figure compared to PYTHIAcalculations. For kaons and protons the positive particle is indicated by the square (red) points and by the open circle (Blue) for the negatives. The data are from 200 GeV $p+p$.

specie	62.4 GeV	200 GeV		
	RMS	Pythia	RMS	Pythia
π^+	1.93 ±0.2	2.01	2.40±0.1	
π^-	1.78±0.2	1.83	2.34±0.2	
K^+	1.67± 0.05	1.68	2.33±0.2	
K^-	1.49±0.04	1.53	2.20±0.2	
$\bar{\text{p}}$	1.19±0.01	1.38	1.90± 0.2	

TABLE VII. Extracted RMS for 62.4 and 200 GeV rapidity distributions compared to RMS from PYTHIAcalculation errors need evaluation and systematic estimate too.

ments of transverse momentum spectra we have yielded rapidity densities. From these we have extracted 4π multiplicities as well as demonstrated longitudinal scaling over $\sqrt{s}$ ranging from 17 to 200 GeV. The longitudinal scaling shows itself in net proton dN/dy distributions as well as net baryon dN/dy distributions. Using transformations of dN/dx_f from 17 GeV to 62.4 and 200 GeV to dN/dy we have shown that dN/dx_f is constant over that range and that the average rapidity loss from $\sqrt{s}$ = 17 to $\sqrt{s}\sim$ 200 GeV remains constant near 0.8.

Comparisons of the data with various models is presented. Comparisons to PYTHIA show broad agreement with the data at $\sqrt{s}$ = 200 GeV, but not so well at 62.4 GeV failing to reproduce the energy dependence. The RMS of the rapidity distributions agrees between model and data for pions, kaons and anti-protons. The pion and kaon distribution are reasonable well described, while severe discrepancy with net-proton distributions exists. Comparisons NLO pQCD calculations to the data at selected rapidities shows that π^+ and π^- are well described while the differences in production between K^+ and K^- in the data are not reproduced by the calculation.

Should we have a comment why NLO may be appropriate even though the soft processes from pythia described data well up to several GeV/c

Ratios of p/π^+, $\bar{p}/\pi^-$, K^+/π^+ and K^-/π^- as a function of p_t show an evolution with rapidity. Ratios of $K^/\pi^+$ and K^-/π^- versus $\bar{p}/p$, a measure of the baryo-chemical potential, show a relationship with the $K^/\pi^+$ and K^-/π^- ratios reaching similar values to those measured in the Au + Au system for the lowest baryo-chemical potential (largest value of $\bar{p}/p$).

VI. ACKNOWLEDGMENTS

We thank the staff of the Collider-Accelerator and Physics Departments at BNL for their vital contributions. We thank Werner Vogelsang for providing us

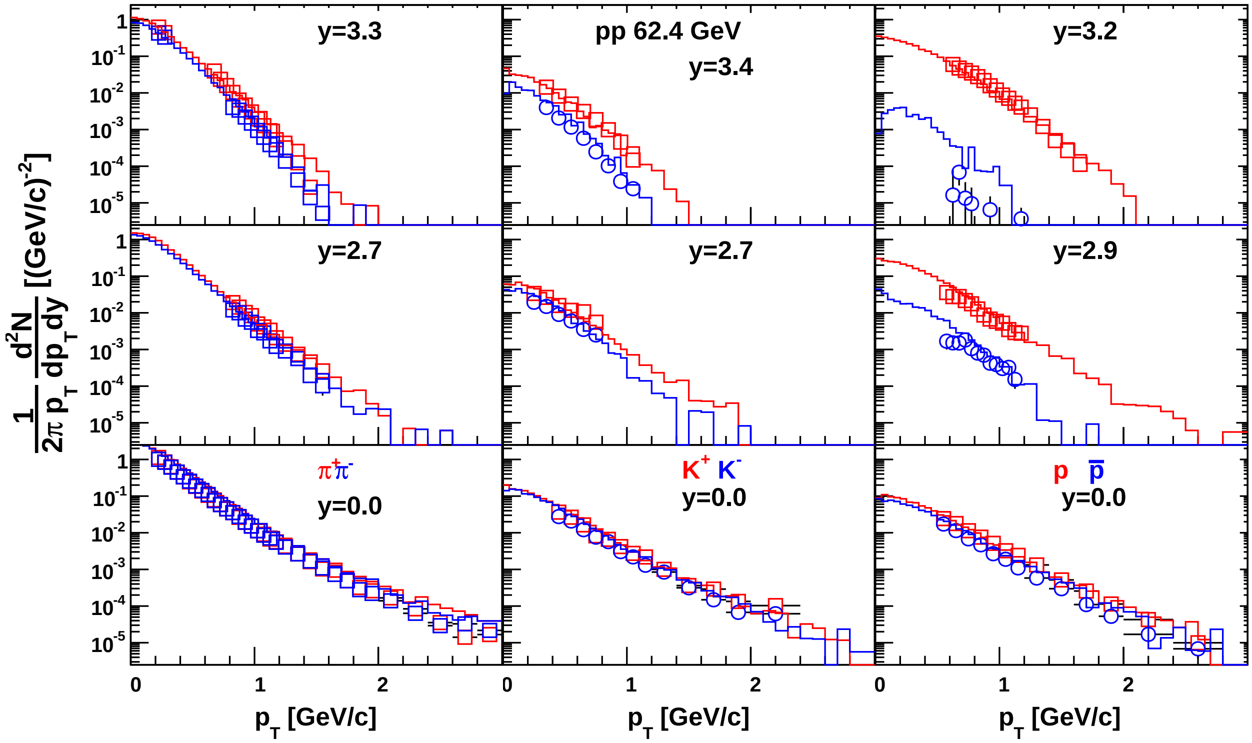

FIG. 27. (Color online) Invariant transverse spectra for π^+, K^+, K^-, p and $\bar{\text{p}}$ at y=0 and at two high rapidities as indicated in the figure compared to PYTHIAcalculations. For kaons and protons the positive particle is indicated by the square (red) points and by the open circle (Blue) for the negatives. The data are from 62.4 GeV $p+p$.

with the NLO pQCD calculations and Daniel DeFlorian for the NLL calculations used in this paper. We also thank Peter Skands, Torbjoern Sjøstrand, and Christine Adelaide for illuminating discussions and advice. This work was supported by the Division of Nuclear Physics of the Office of Science of the U.S. Department of Energy under contracts DE-AC02-98-CH10886, DE-FG03-93-ER40773, DE-FG03-96-ER40981, and DE-FG02-99-ER41121, the Danish Natural Science Research Council, the Research Council of Norway, the Polish Ministry of Science and Higher Education (Contract no 1248/B/H03/2009/36), and the Romanian Ministry of Education and Research for the grant no.81-049/2007 (REEHUC)" and a sponsored research grant from Renaissance Technologies Corp.

---

[1] I. Arsene *et al.* (BRAHMS), Nuclear Physics A **757**, 1 (2005).

[2] B. B. Back *et al.* (PHOBOS), Nuclear Physics A **757**, 28 (2005).

[3] J. Adams *et al.* (STAR), Nucl. Phys. **A757**, 102 (2005), nucl-ex/0501009.

[4] K. Adcox *et al.* (PHENIX), Nucl. Phys. **A757**, 184 (2005), nucl-ex/0410003.

[5] S. S. Adler *et al.* (PHENIX), Phys. Rev. Lett. **95**, 202001 (2005), arXiv:hep-ex/0507073.

[6] J. Adams *et al.* (STAR), Phys. Lett. **B612**, 181 (2005), arXiv:nucl-ex/0406003.

[7] I. Arsene *et al.* (BRAHMS), Phys. Rev. Lett. **98**, 252001 (2007), arXiv:hep-ex/0701041.

[8] B. I. Abelev *et al.* (STAR), Physical Review Letters **101**, 222001 (2008).

[9] D.L.Adams *et al.* (E704 Collaboration), Phys. Lett. **B264**, 462 (1991).

[10] A.Bravar *et al.* (E704 Collaboration), Phys. Rev. Lett. **77**, 2626 (1996).

[11] I. Arsene *et al.* (BRAHMS), Phys. Rev. Lett. **101**, 042001 (2008), arXiv:0801.1078 [nucl-ex].

[12] J. H. Lee and F. Videbaek (BRAHMS), AIP Conf. Proc. **915**, 533 (2007).

[13] U. D'Alesio and F. Murgia, Phys. Rev. **D70**, 074009 (2004), hep-ph/0408092.

[14] T. Sjostrand *et al.*, Comput. Phys. Commun. **135**, 238 (2001), arXiv:hep-ph/0010017.

[15] T. Sjostrand, S. Mrenna, and P. Skands, JHEP **05**, 026 (2006), arXiv:hep-ph/0603175.

[16] P. Z. Skands, Phys. Rev. D **82**, 074018 (2010).

[17] R.Debbe *et al.* (BRAHMS Collaboration), Nucl. Instr. Meth. **A570**, 216 (2007).
[18] M.Adamczyk *et al.* (BRAHMS Collaboration), Nucl. Instr. Meth. **A499**, 437 (2003).
[19] I.Arsene *et al.* (BRAHMS Collaboration), Phys. Review C **A570**, 216 (2005).
[20] B.Budick *et al.*, Nuclear Inst. and Methods in Physics Research **A621**, 295 (2010).
[21] A. Drees, Z. Xu, B. Fox, and H. Huang, in *Particle Accelerator Conference, 2003. PAC 2003. Proceedings of the*, Vol. 3 (2003) pp. 1688 – 1690 vol.3.
[22] S. S. Adler *et al.* (PHENIX), Phys. Rev. Lett. **91**, 241803 (2003), arXiv:hep-ex/0304038.
[23] *GEANT program library*.
[24] R. J. S. P. Fasso A., Ferrari A., in *Proc. IV Int. Conf. on Calorimetry in High Energy Physics, La Biodola (Italy)*, edited by E. A. Menzione and A. Scribano (World Scientific, 1993) pp. 493–502.
[25] P.H.Christiansen, Ph.D. Thesis, University of Copenhagen (2003).
[26] B. I. Abelev *et al.* (STAR), Phys. Rev. **C75**, 064901 (2007), arXiv:nucl-ex/0607033.
[27] I. G. Bearden *et al.* (BRAHMS Collaboration), Phys. Rev. Lett. **93**, 102301 (2004).
[28] D. Drijard *et al.* (CERN-Dortmund-Heidelberg-Warsaw Collaboration), Z.Phys. **C12**, 217 (1982).
[29] I. G. Arsene *et al.* (BRAHMS), Phys. Lett. **B684**, 22 (2010), arXiv:0910.3328 [nucl-ex].
[30] B. Alper *et al.* (British-Scandinavian), Nucl. Phys. **B100**, 237 (1975).
[31] K. Guettler *et al.* (British-Scandinavian-MIT), Phys. Lett. **B64**, 111 (1976).
[32] B. Alper *et al.*, Phys. Lett. **B47**, 275 (1973).
[33] K. Guettler *et al.* (British-Scandinavian-MIT), Nucl. Phys. **B116**, 77 (1976).
[34] M. Banner *et al.*, Nucl. Phys. **B126**, 61 (1977).
[35] A. Adare *et al.* (PHENIX), Phys. Rev. **C83**, 064903 (2011), arXiv:1102.0753 [nucl-ex].
[36] M. Albrow *et al.*, Nucl. Phys. **B56**, 333 (1973).
[37] B. I. Abelev *et al.* (STAR), Phys. Rev. **C79**, 034909 (2009), arXiv:0808.2041 [nucl-ex].
[38] G. J. Alner *et al.* (UA5), Z. Phys. **C33**, 1 (1986).
[39] B. Alver *et al.* (PHOBOS), Phys. Rev. **C83**, 024913 (2011), arXiv:1011.1940 [nucl-ex].
[40] G. Wilk and Z. Wlodarczyk, Phys. Rev. Lett **84**, 2770 (2000).
[41] J. Adams *et al.* (STAR), Phys. Rev. C **71**, 064902 (2005).
[42] A. Adare *et al.* (PHENIX), (2010), arXiv:1005.3674 [hep-ex].
[43] J. Benecke, T. T. Chou, C. N. Yang, and E. Yen, Physical Review **188**, 2159 (1969).
[44] C. Alt *et al.* (NA49), Eur. Phys. J. **C45**, 343 (2006), hep-ex/0510009.
[45] T. Anticic *et al.* (NA49), Eur. Phys. J. **C65**, 9 (2010), arXiv:0904.2708 [hep-ex].
[46] W. Busza and A. S. Goldhaber, Phys.Lett. **B139**, 235 (1984).
[47] I. G. Bearden *et al.* (BRAHMS Collaboration), Phys.Rev.Lett. **93**, 102301 (2004), arXiv:nucl-ex/0312023 [nucl-ex].
[48] I. Arsene *et al.* (BRAHMS Collaboration), Phys.Lett. **B677**, 267 (2009), arXiv:0901.0872 [nucl-ex].
[49] M. Antinucci *et al.*, Lett. Nuovo Cim. **6**, 121 (1973).
[50] M. Aguilar-Benitez *et al.*, Z. Phys. **C50**, 405 (1991).
[51] A. Breakstone *et al.* (Ames-Bologna-CERN-Dortmund-Heidelberg-Warsaw Collaboration), Phys.Rev. **D30**, 528 (1984).
[52] A. Adare *et al.* (PHENIX), Phys. Rev. **D79**, 012003 (2009), arXiv:0810.0701 [hep-ex].
[53] D. de Florian, R. Sassot, and M. Stratmann, Physical Review D **75**, 114010 (2007).
[54] C.Bourrely and J.Soffer, Eur.Phys.J **J36**, 371 (2004).
[55] Owen *et al.*, Phys. Rev. Lett. **45**, 89 (1980).
[56] I. Arsene *et al.* (BRAHMS Collaboration), Phys.Lett. **B687**, 36 (2010), arXiv:0911.2586 [nucl-ex].
[57] Z.-B. Kang and F. Yuan, (2011), * Temporary entry *, arXiv:1106.1375 [hep-ph].
[58] I. Otterlund *et al.*, Nuclear Physics B **142**, 445 (1978).
[59] S. S. Adler *et al.* (PHENIX), Phys. Rev. **C74**, 024904 (2006), arXiv:nucl-ex/0603010.
[60] J. Adams *et al.* (STAR), Phys. Rev. Lett. **91**, 072304 (2003), arXiv:nucl-ex/0306024.
[61] B. B. Back *et al.* (PHOBOS), Phys. Rev. Lett. **91**, 072302 (2003), arXiv:nucl-ex/0306025.
[62] S. S. Adler *et al.* (PHENIX), Phys. Rev. Lett. **91**, 072303 (2003), arXiv:nucl-ex/0306021.
[63] B. Jager, A. Schafer, M. Stratmann, and W. Vogelsang, Physical Review D **67**, 054005 (2003).
[64] Z.-W. Lin, C. M. Ko, B.-A. Li, B. Zhang, and S. Pal, Phys. Rev. **C72**, 064901 (2005), arXiv:nucl-th/0411110.
[65] H. Petersen, M. Bleicher, S. A. Bass, and H. Stocker, (2008), arXiv:0805.0567 [hep-ph].
[66] I. Arsene *et al.* (BRAHMS), Phys. Rev. Lett. **91**, 072305 (2003), arXiv:nucl-ex/0307003.
[67] A. Breakstone *et al.* (Ames-Bologna-CERN-Dortmund-Heidelberg-Warsaw), Z. Phys. **C69**, 55 (1995).
[68] B. Alper *et al.* (British-Scandinavian ISR), Phys. Lett. **B44**, 521 (1973).
[69] B. Alper *et al.* (British-Scandinavian ISR), Phys. Lett. **B44**, 527 (1973).
[70] B. Alper *et al.*, Phys. Lett. **B47**, 75 (1973).
[71] D. d'Enterria, J.Phys **G31**, S491 (2005).
[72] B. I. Abelev *et al.* (STAR), Phys. Rev. Lett. **97**, 152301 (2006), arXiv:nucl-ex/0606003.
[73] P. Eden and G. Gustafson, Z. Phys. **C75**, 41 (1997), arXiv:hep-ph/9606454.
[74] J. Adams *et al.* (STAR), Phys. Rev. Lett. **97**, 152302 (2006), arXiv:nucl-ex/0602011.
[75] F. W. Bopp, J. Ranft, R. Engel, and S. Roesler, Physical Review C (Nuclear Physics) **77**, 014904 (2008).
[76] G. E. Cooper (NA49), Nucl. Phys. **A661**, 362 (1999).
[77] K. e. Aamodt (ALICE Collaboration), Phys. Rev. Lett. **105**, 072002 (2010).